The mixed-bed glacial landform imprint of the North Sea Lobe in the western North Sea

David H. Roberts[1*], Elena Grimoldi[1], Louise Callard[1], David J.A.Evans[1], Chris D. Clark[2], Heather A. Stewart[3], Dayton Dove[3]; Margot Saher[4], Colm Ó Cofaigh[1], Richard C. Chiverrell[5], Mark D.Bateman[2], Steven G. Moreton[6], Tom Bradwell[7], Derek Fabel[8], Alicia Medialdea[9].

[1] Department of Geography, Durham University, Durham, DH1 3LE, UK
[2] Department of Geography, University of Sheffield, Sheffield, S10 2TN, UK
[3] British Geological Survey, Lyell Centre, Research Avenue South, Edinburgh, EH14 4AP, UK
[4] School of Ocean Sciences, Bangor University, Menai Bridge, LL59 5AB, UK
[5] Department of Geography, University of Liverpool, Liverpool, L69 7ZT, UK
[6] Natural Environment Research Council, Radiocarbon facility, East Kilbride, Scotland, G75 OQF, UK
[7] Biological and Environmental Sciences, University of Stirling, Stirling, Scotland, FK9 4LA, UK
[8] SUERC, Rankine Avenue, Scottish Enterprise Technology Park, East Kilbride, G75 0QF, UK
[9] Geography Insitute, University of Cologne, Otto-Fischer-Str. 4 50674 Cologne, Germany

*Correspondence to: David H. Roberts, Department of Geography, Durham University, Durham, DH1 3LE, UK. Email: D.H.Roberts@durham.ac.uk

---

ABSTRACT: During the last glacial cycle an intriguing feature of the British-Irish Ice Sheet was the North Sea Lobe (NSL); fed from the Firth of Forth and which flowed south and parallel to the English east coast. The controls on the formation and behaviour of the NSL have long been debated, but in the southern North Sea recent work suggests the NSL formed a dynamic, oscillating terrestrial margin operating over a deforming bed. Further north, however, little is known of the behaviour of the NSL or under what conditions it operated. This paper analyses new acoustic, sedimentary and geomorphic data in order to evaluate the glacial landsystem imprint and deglacial history of the NSL offshore from NE England.

Subglacial tills (AF2/3) form a discontinuous mosaic interspersed with bedrock outcrops across the seafloor, with the partial excavation and advection of subglacial sediment during both advance and retreat producing mega-scale glacial lineations and grounding zone wedges. The resultant 'mixed-bed' glacial landsystem being the product of a dynamic switch from a terrestrial piedmont-lobe margin with a net surplus of sediment to a partially erosive, quasi-stable, marine-terminating, ice stream lobe as the NSL withdrew northwards.

Glaciomarine sediments (AF4) drape the underlying subglacial mixed-bed imprint and point to a switch to tidewater conditions between 19.9 and 16.5ka cal BP as the North Sea became inundate. The dominant controls on NSL recession during this period were changing ice flux through the Firth of Forth ice stream onset zone and water depths at the grounding line; the development of the mixed-bed landsystem being a response to grounding line instability.

KEYWORDS: British-Irish Ice Sheet; North Sea Lobe; ice stream onset; mixed-bed glacial landform assemblage

Introduction

During the last glacial cycle, the North Sea Basin (NSB) was overrun at various times both by the British-Irish Ice Sheet (BIIS) and the Fennoscandian Ice Sheet (FIS). As such it was an area characterised by complex ice sheet dynamics resulting from ice sheet coalescence, decoupling, ice divide migration, marine inundation and the switching on and off of ice streams (Graham et al., 2007, 2011; Sejrup et al., 2016; Patton et al., 2017). A particularly intriguing glaciological attribute of ice sheet inundation of the NSB was the formation of the North Sea Lobe (NSL), nourished by ice emanating from Northern England and Scotland, flowing south and parallel to the English east coast and periodically surging (Boulton et al, 1977; Eyles et al; 1994; Boston et al., 2010) (Fig. 1). The vast majority of the evidence for the NSL has been derived from onshore glaciogenic sediment exposures, ice marginal geomorphology and palaeo-ice dammed lakes (Wood and Rome; 1868; Lamplugh; 1879, Bisat, 1932; Eyles et al., 1982; Evans et al., 1995; Catt 2007; Bateman et al., 2008, 2011, 2015, 2017; Evans and Thomson; 2010; Davies et al., 2009, 2012; Roberts et al. 2013), however, few studies (with the exception of Davies et al., 2011; Dove et al., 2017) have focussed on the offshore imprint of the NSL .

The flow trajectory of the NSL offshore has been correlated with the offshore subglacial footprint of the Wee Bankie and Bolders Bank Formations (Boulton et al., 1985; Balson and Jeffrey, 1991; Cameron et al., 1992; Gatliff et al., 1994; Carr et al., 2006; Davies et al., 2011)(Fig. 1), both thought to have been deposited during the last glacial cycle and often associated with the Dimlington Stade and the later onshore deposition of the Skipsea and Withernsea tills (Bateman et al, 2011; 2017). Recently, Dove et al. (2017) have demonstrated that multiple tills associated with the Bolders Bank Formation form distinctive off-lapping sheets or arcuate moraines across the seafloor. They mark the northwards recession of the NSL from the Norfolk coast back towards North Yorkshire after 22.8 – 21.5 ka (Roberts et al., 2018).

The stratigraphic architecture of the till sheets and moraines suggest a dynamic, oscillating margin operating over a deforming bed, with tunnel valleys indicating a surplus of meltwater during deglaciation (Dove et al, 2017). Further north, however, in the area offshore from Durham and Northumberland, very little is known of the glaciogenic imprint of the NSL across the seafloor. The Wee Bankie Formation has been interpreted as a subglacial till, and the St Abbs, Forth, and Sunderland Ground formations as deglacial phase glaciomarine sediment (Cameron et al., 1992; Gatliff et

al., 1994) (Fig. 2), but the geomorphic imprint of the NSL and its recessional history have not been adequately constrained. Given the NSL was sourced from central Scotland via the Firth of Forth and the influence of the NSL on the BIIS in terms of ice divide migration, ice drawdown and flow trajectory would have been significant, particularly during deglaciation (Roberts et al. 2018). Yet it remains unclear as to whether the NSL behaved as an ice stream, a terrestrial piedmont lobe or a tidewater terminating glacier (Golledge and Stoker, 2006; Boston et al. 2010; Dove et al. 2017). Thus a better understanding of the NSL's duration, style and retreat pattern is important not only to reconstruct BIIS dynamics but also to the development of robust ice sheet models.

This paper analyses acoustic, sedimentary and geomorphic data collected by the BRITICE-CHRONO project and collated under the Glaciated North Atlantic margins (GLANAM) project in order to evaluate the glacial landsystem imprint of the NSL offshore from Durham and Northumberland. Furthermore, it assesses evidence for a subglacial to glaciomarine transition during deglaciation, and establishes the timing of deglaciation offshore as ice moved back towards the Firth of Forth.

Regional setting

The study area is situated offshore of the Durham and Northumberland coasts, and runs from Eyemouth in the north to Sunderland in the south (Figs. 1, 2). It covers around 25,000 km^2 of the seabed. The region is underlain by Carboniferous, Permian and Triassic rocks (Fig. 2a) (Cameron et al., 1992), above which several Quaternary glaciogenic formations have been mapped. Immediately offshore, the Quaternary sediments are thin, with bedrock commonly exposed at the seabed. Beyond 15km offshore the Quaternary sediments begin to thicken eastward. With respect to the last glacial cycle they include the Wee Bankie Formation, which is interpreted as subglacial in origin and probably contiguous with Bolders Bank Formation further south (Fig. 2b; Stoker and Bent, 1985; Gatliff et al., 1994). It is composed of stiff diamicton with interbeds of sand, pebbly sand and silty clay (Cameron et al., 1992; Gatliff et al., 1994; Davies et al., 2011). The Forth Formation is variously described as a series of marine, glaciomarine, fluviomarine and estuarine sediments. It occurs in pockets across the seafloor (Cameron et al., 1992; Gatliff et al., 1994). The St Andrews Bay and Largo Bay Members are related to the Forth Fm, and the St Abbs and Sunderland Ground

Formations also probably represent deglacial glaciomarine conditions with transitions to upper Holocene marine sediments (Fig. 2b). An alternative explanation for the Sunderland Ground Fm is deposition in a glaciolacustrine environment as an extension of glacial lake Wear (Catt, 2007).

Glacial sediments deposited by the NSL can also be found along the Northumberland and Durham coasts. The lower diamicton of the Warren House Formation is an MIS 8 to 12 glaciomarine deposit and was renamed the 'Ash Gill Member' (Davies et al. 2012b). The Blackhall and Horden Till Formations and the Peterlee Sand and Gravel Formation along the Durham coast date to MIS 2 (Davies et al., 2009, 2012a). The Blackhall Till Formation originated in north-western England and was deposited by the Tyne Gap Ice Stream (Davies et al., 2009), but the Horden Till was deposited by the NSL with ice originating from Scotland and moving south via the Cheviots and Northumberland coast (Everest et al., 2005; Davies et al., 2009; Livingstone et al., 2012). Glaciolacustrine sediments associated with glacial lakes Wear and Tees also crop out at the coast and may be contiguous with the Sunderland Ground Formation offshore. The ice marginal geomorphic imprint of the NSL pushing onshore can be discerned in a series of linear kames, moraines, eskers and ice dammed lake basins that run north to south from Berwick-upon-Tweed to the Tees (Livingstone et al., 2015; Teasdale, 2013).

The imprint of the NSL offshore with respect to both ice advance and retreat is poorly constrained. The footprint of the Wee Bankie Formation may be contiguous with the Bolders Bank Formation further south, and if so, the Wee Bankie Formation sediments may mark the passage of the NSL during both advance and recession along the north coast of England during the last glacial cycle (Balson and Jeffrey, 1991; Carr et al., 2006). It is most likely that the NSL was fed by ice from Scotland through the Firth of Forth which may have acted as an ice stream onset zone (Golledge and Stoker, 2006; Hubbard et al., 2009), though in the southern NSB the geomorphic imprint of the NSL and the association of subglacial and glaciofluvial sediments points to a terrestrial piedmont lobe (Dove et al., 2017). During deglaciation, optically stimulated luminescence samples (OSL) from Norfolk show the ice first receded northwards after 21.5ka (Roberts et al., 2018) and that ice departed the Yorkshire coast as late as ~ 17.6ka (Bateman et al., 2017; Evans et al. 2017). Livingstone et al. (2015) propose deglaciation of the area west of Newcastle at 17.8 to 17.6ka based on Be^{10} exposure ages. Finally, there are multiple dates around the edges of the Firth of Tay and Firth of

Forth which suggest ice had retreated into that part of Scotland by 17.0 – 16.5 cal. ka BP with glaciomarine environments on-lapping the present coast (Peacock, 2002). These ages suggest a window of recession of ~1000yrs for the NSL between Yorkshire and the Firth of Forth towards the end of the Last Glacial Maximum (LGM) (Fig. 1).

Methods

The bathymetric data included in this paper where downloaded from the UK Hydrographic Office (UKHO) under the Open Government Licence v3 and cover an area which extends up to ~125 km from the coastline, from Eyemouth in the north to Sunderland in the south (Fig. 3a). A Digital Elevation Model (DEM) of the UKHO data was created at 50m horizontal resolution. An area of multibeam bathymetry data located approximately 11 km off the Northumberland coast, covering an area of approximately 705 km^2 was provided courtesy of Defra. A DEM of the Defra data was created at 5 m resolution. The GEBCO 2014 grid and Olex database for the North Sea (www.olex.no) were also used to provide regional bathymetric information for the western North Sea. The combined bathymetric surfaces were used for geomorphological interpretation.

The shallow sub-seabed geology was interpreted from a mixture of sub-bottom profiler (chirp) data collected during cruise JC123 onboard the RRS James Cook in August 2015, and digital scans of single-channel seismic (surface tow boomer and sparker) data acquired by the British Geological Survey from the 1970s to 1990s (Fannin, 1989). Chirp data was collected using a hull mounted Kongsberg SBP-120 sub-bottom profiler that operated a sweep frequency of between 2500 to 6500 kHz with a depth resolution of 0.3 ms. All seismic data were interpreted using the IHS Kingdom™ software.

Seven vibrocores are described in detail. They were retrieved using the British Geological Society vibrocorer with a 6 m barrel and 8 cm core diameter. The cores were measured for magnetic susceptibility (MS) and gamma density, using Geotek Multi-Sensor Core Logger (MSCL) at two centimetre resolution. A Geotek XCT scanner provide X-radiographs. Shear vane measurements using a hand held Torvane was carried out on-board. Sedimentary facies are described following Evans and Benn (2004). These cores are supplemented by unpublished data from core 118VC from the area west of the Firth of Forth and a glacial sediment section from the coast at Seaham.

Both sites provide additional onshore/offshore context relating to regional deglacial history.

Micropalaeontological analysis on foraminifera was attempted on all the cores. Each sample was wet sieved through 500 µm and 63 µm sieves. Foraminifera were dry picked from the 63 to 500 µm fractions under a Zeiss Stemi SV11 binocular microscope. Studies on benthic foraminifera species for paleoenvironmental reconstructions usually require a minimum of 300 individuals to obtain a reliable indicator of the species diversity (Jennings et al., 2014). However, due to low species abundance only two sample counts were >200 with the majority of counts less than 100. The foraminifera assemblages instead provide an indication of the depositional palaeoenvironment.

A total of five radiocarbon samples, including one bivalve and four mixed benthic foraminifera samples, from four cores (118VC, 128VC, 132VC and 137VC), were submitted for analysis. The whole bivalve was cleaned with deionised water and dried at 40°C. The foraminifera samples were dry picked from the 500 and 63 µm fractions. The samples were submitted to the NERC radiocarbon facility in East Kilbride where they were hydrolysed to CO_2 using 85% orthophosphoric acid at room temperature and reduced to graphite using a two-stage reduction over heated Zn and Fe (Slota et al., 1987). The prepared graphite targets were passed to the SUERC AMS laboratory (SUERC publication codes) or the Keck C Cycle AMS laboratory, University of California, Irvine (UCIAMS publication codes) for ^{14}C measurement. The conventional ages were calibrated using OxCal 4.2 calibration programme (Bronk Ramsey 2009) with the Marine13 curve, an inbuilt marine reservoir correction of 400 years and a ΔR of 0 years (Reimer et al., 2013). The ages are reported in the text as the calibrated 2σ median result (Table 1). Only the calibrated ΔR of 0 are used in the text.

Three sand samples from glaciofluvial facies exposed on the coast at Seaham were collected in opaque pvc tubes for optically stimulated luminescence (OSL) dating (Table 2). These were prepared following standard procedures to isolate and clean the quartz fraction (see Bateman and Catt, 1996). Dose rates were based on radionuclide concentration determined by inductively couple plasma mass spectroscopy for the beta dose rate contribution and in situ gamma spectrometry for the gamma dose rate. A cosmic dose rate was calculated based on average burial depths through time using the algorythmn of Prescott and Hutton (1994). Dose rates were appropriately attenuated for

grain size and palaeomoisture. The latter were estimated at 23% to reflect the stratigraphic positions of the sand unit sampled in an aquiclude between two diamicts. OSL measurements used an automated Risø readers with blue (470 nm) LEDs and were on ultra-small multigrain aliquots (SA, containing 20 grains each). All samples were measured using the SAR protocol (Murray and Wintle, 2003) including an IR depletion ratio step to test for feldspar contamination and a preheat of 220 °C for 10 s. The latter was derived experimentally from a dose recovery preheat test. For each sample, 60-92 SA replicates were measured. Derived D_e estimates were accepted if the relative uncertainty on the natural test dose response was <20%, the recycling and the IR depletion ratio (including uncertainties) were within 20% of unity and recuperation <5%.

The resulting OSL data showed D_e distributions were non-normal and too highly scattered (over-dispersion ranged from 72-83%) to be considered as belonging to well bleached sediments. As a result the internal-external consistency model (IEU, Thomsen et al., 2007) was adopted to derive an estimate the true (bleached) burial dose with the starting parameters based the results from the well bleached samples from Heslerton (See Evans et al 2017 for details). Such an approach has been shown to be appropriate to estimate accurate ages for incompletely bleached glacial sediments (Bateman et al., 2017). Ages are reported in Table 2 calculated from the time of measurement (2013) with one sigma uncertainties.

Results

Regional bathymetry and seismic data

The area offshore from Durham and Northumberland is very shallow (Fig. 3a). To the north, water depths do not exceed ~ -80 m. Further south, waters are up to 40 m deep along the coastline but deepen eastward and average ~ -70 m. However, local basins in the central part of the study area reach a maximum depth of -113 m. (Fig. 3a). Where the seafloor is relatively smooth it is covered by soft sediment. In other areas, bedrock is close to, or at, the seafloor (Figs. 3a, 3b).

Five different acoustic facies were mapped across the study area (Figs. 4 and 5). AF1 is the lowermost facies of the sequence and is composed of mainly of Permian bedrock,

though Triassic, Cretaceous and Jurassic rocks are present in the study area (Cameron et al., 1992; Gatliff et al., 1994) (Figs. 2, 5a, 5b). Bedrock is generally present at very shallow depths below the seabed, forming the distinctive topography of the seafloor. It is often heavily folded and faulted with strata orientated sub-vertically in many areas (Fig. 5a). There are also several intrusive complexes forming ridges on the seafloor, with ridges R6 and R11 being particularly clear examples (Fig. 4a). There are four acoustic facies that can be mapped above the bedrock (AF2 – AF5). They have a patchy distribution across the study area, being laterally discontinuous and of variable thickness (Figs. 4, 5).

AF2 is laterally discontinuous and relatively thin, occurring only as isolated lenses of sediment (Fig. 4). On average it is 2–6 m thick and lies directly on bedrock. It is internally transparent and structureless but its upper surface is often characterised by low amplitude, irregular bumps (e.g. Fig. 5a). AF3 is the most ubiquitous facies in the study area and occurs over the bedrock or lenses of AF2. AF3 exhibits variable thickness, being thickest (10-25 m) where it forms the core of wedges W1 and W2 (Figs. 4a, 4b). Between W1 and W2 it thins in places to only 1-2 m, and often disappears over bedrock bedforms. In some locations (irrespective of the underlying bedrock) AF3 is characterised by an undulatory, upper surface (Fig. 5a). Internally, the facies is often slightly more opaque than AF2 and structureless, with the exception of occasional chaotic reflectors.

AF4 overlies AF3, although it occasionally lies directly on top of bedrock strata. Its acoustic appearance is defined by high frequency, parallel sub-horizontal reflectors (Fig. 5a). It often infills small depressions and basins (Fig. 4), and hence thickens and thins across the study area. At its thickest it is 8-10m, although in the south and west basins it deepens to 20-25 m. In Figure 5a the internal reflectors within AF4 are wavy and appear to mimic the underlying ‘bumpy’ surface of AF3. The upper boundary of AF4 is usually flat. AF5 is the uppermost facies of the seismic sequence. It is thin, laterally discontinuous and difficult to map where bedrock is close to the seafloor. It is acoustically transparent on seismic profiles (Figs. 4, 5, 6)

Sediment cores

Seven vibrocores from the study are described in detail (128VC, 132VC, 133VC, 134VC, 135VC, 136VC, 137VC).

Core 128VC is located to the north of our study area (Fig. 3a, 4a). It is 4.5 m long and captures both AF3 and AF4, which directly overlay Carboniferous (Dinantian) bedrock (Figs. 6 and 7a). The basal 59 cm is a brown, matrix supported, diamict (Dmm; AF3) containing abundant sub-rounded to sub-angular clasts in a silty matrix. Shear strengths increase downwards from 18 kPa to 68 kPa. Magnetic suspectibility (MS) is also high and increases with depth (see Supplementary information). The lower Dmm is transitional upwards to a stratified diamict (Dms) between 400–360cm, with sorted, planar horizontal, draped laminae becoming interspersed with diamictic material. The lower Dms is transitional to 72 cm thick laminated silt and clay unit (Fl); Fig. 7a), which in turn is overlain by 236 cm of soft (<10 kPa), colour banded clay that is occasionally laminated and contains thin sandy silt lenses (Fl/Sl; AF4). The core is capped by ~ 80 cm of shelly, silty sand with shell fragments increasing in abundance down core (AF5). One mixed benthic foraminifera sample from 280 cm down core in the (laminated silt and clay) provided a radiocarbon age of 16,949 ± 216 cal. BP (Table 1). Samples for foraminifera analysis where taken at 20 cm resolution below 60 cm in the core. There were no foraminifera present in the Dmm and only low abundance in the Fl unit, with the species assemblage dominated by Elphidium clavatum.

Core 132VC is located approximately 20 km south-west of R11 (Fig. 3a, 4a) and was collected from a trough adjacent to a bedrock-cored lineation. Seismic data suggest the core sampled a lens of AF4 though it did not penetrate AF3 (Fig. 6). Permian strata are present underneath the Quaternary sediments at this location. The base of core 132VC is characterised by 79 cm of very soft, laminated silty clay, which contains clear colour banding from red to brown, occasional 0.5-1 cm thick silt bands and outsize clasts (Fig. 7b; Fl(d)). The Fl(d) is overlain by 26 cm of dark grey/brown, soft, matrix supported Dmm that contains abundant clasts within a silty clay matrix. MS and gamma density are both high in the Dmm (see supplementary information. The Dmm is overlain by a, soft, massive, brown clay (Fm) that contains the occasional silt/fine sand lenses. This Fm unit is truncated by a 16 cm layer of gravelly, silty, sand (Sm/Glag) with abundant shell valves and fragments. The top 54 cm of the core consists of dark brown, massive, silty sand (Sm), with occasional presence of shell fragments.

Foraminifera analysis was restricted to the Fl(d) and Fm lithofacies in core 132VC. No tests were present below 209 cm. The remaining samples contained low foraminifera abundance (<150 tests per sample) with the assemblage dominated by Elphidium clavatum with Haynesina obiculare a secondary species. E. albiumbilicatum, E. askulundi and E. excavatum are also present in low abundance with Cassidulina reniforme appearing with minor counts at 84 cm. One radiocarbon sample from benthic foraminifera was taken at 144 cm down core, directly below the lower contact of the Dmm, within the Fl(d) unit. It returned a radiocarbon age of 19, 571 ± 172 cal. BP (Fig. 7b; Table 1).

Core 134VC is located just offshore from Newcastle (Fig. 3a, 4b) and is 4.5 m long. The core base is a massive, brown, matrix supported Dmm. It has a sandy, silty, clay matrix with abundant clasts of varying lithologies and a shear strength ranging from 20 - 25 kPa. It corresponds to AF3 as identified in the geophysical survey (Fig. 6). The Dmm has some subtle stratification and a gradational upper contact to a brown/red, soft, massive clay with occasional outsize clasts (Fl(d)). This unit is colour banded, and there are occasional silt laminae, granules and clasts. It is part of AF4 (Fig. 6). A disturbed layer marks the upper contact and transition to a poorly sorted, gravelly, coarse sand (Sm) with shell fragments which is gradational to a moderately sorted, silty, sand (Sm), with small shell fragments; this corresponds to AF5 (Fig. 6).

Core 133VC is located 20 km south of 134VC but has very similar sedimentology. At its base (333 – 424 cm) it is characterised by a soft brown diamict that becomes partially stratified up core (Dms), with laminations of sorted silt/clay towards becoming more frequent towards the upper contact boundary. The Dms is sharply overlain by 2 m of a brown/reddish laminated clay/silt unit with clasts and dropstones (Fl(d)). Laminae are occasional tilted and disturbed. Clast abundance decreases up core and lamination becomes thinner (sub 1mm) and more frequent; they eventually fade out. The core is capped by a shell hash and massive grey sand with shell fragments.

Core 135VC is 5.66 m long and is situated in a bathymetric low approximately 72 km east of Sunderland (Fig. 3a, 4a, 4b). At its base is a reddish brown, massive, stiff (40-70 kPa) diamict (Dmm) with abundant clasts of different dimensions and lithologies within a silty clay matrix (Fig. 8a). It forms part of AF4 (Fig. 5). Between 494 and 488cm there is a distinctive stratified silt unit and above this the Dmm is crudely colour banded.

Overlying the Dmm is a laminated and colour banded (red/brow/grey) soft, clay silt with small clasts (Fl(d)) (Fig. 8a). Numerous laminae (up to 1 cm in thickness) of reddish brown well sorted, fine sand (Sm) are present throughout the entire unit. This unit is part of AF 4 (Fig. 6). Above the Fl(d) is an 11 cm thick, brown/grey moderately sorted, fine to medium sand layer (Sm), containing abundant shell fragments. The upper unit of the core is characterised by 23 cm of grey, moderately sorted, fine/medium sand (Sm) with shell fragments (AF5). MS data show relatively low and constant values throughout the core until a visible increase just above the top of the diamict (likely due to the presence of larger clasts; see supplementary information).

Core 135VC was found to have foraminifera preserved within the sediment although in low abundance throughout (no foraminifera were present in the Dmm). The Fl(d) is characterised by low foraminifera abundance with the exception of a sample from 160 cm which is dominated by the species Elphidium clavatum plus other species such as E. incertum, Bolivina inflata and some planktonic species (Fig. 8b). However, there were some notable deviations to this trend with a sample directly overlying the Dmm containing Cibicides lobatulus, and a sample at 376 cm being composed solely of Haynesina obiculare. The uppermost sample was collected at 20 cm depth from within the Sm lithofacies (AF5). It contained a high abundance of quartz fragments and other grains, shell fragments and sea urchin spines, but was devoid of foraminifera.

Core 136VC is 4.05 m long and located approximately 16 km southeast of core 135VC (Figs. 3a, 4a). It comprises a lower unit of interlaminated sand, silts and clays (Fl/Sl) overlain by an upper diamict (Dmm) which is capped by a shelly sand (Sm). The lower Fl/Sl unit is part of AF4 has rapidly alternating laminae with several silty/sand laminae exhibiting bedforms, with planar cross lamination, micro-ripples, and micro cut and fill structures (Fig. 9a). The contact to the overlying Dmm appears gradational and the Dmm(s) is partially stratified in places with thin, well sorted, silty lamina. It has a silt/clay matrix and shear strengths that vary between 50 - 70 kPa. The acoustic imagery from the site appears to show a lens/sheet of sediment off-lapping the north side of the local basin where 136VC is situated (Fig. 4a). The upper 70cm of the core is composed of a silty, coarse sand with abundant shell fragments (AF5).

Core 137VC is 5.66 m long and situated approximately 50 km northeast of 135VC. AF3 was not present at the base of the core. The lowest unit (AF4; 68–566 cm) is composed

mainly of interlaminated silts and sands that fine upwards into silt and clays (Fig. 9b). Laminae become more frequent but thinner up core. A mixed benthic foraminifera sample, with a species assemblage dominated by Elphidium clavatum, from 552 cm provided a radiocarbon age of 19,895 ± 218 cal. BP (UCIAMS-176372; Table 1). The upper unit (0-68 cm) is a dark grey to olive grey silty coarse sand with abundant shell fragments (AF5). The contact between the two units is heavily disturbed with intraclasts of clay pointing to reworking of the lower unit.

Onshore sediments

To provide a tie point for the offshore data (both sedimentologically and geochronologically) additional evidence for NSL glaciation is also presented from Seaham where sands and gravels sit between two diamicts. This site exhibits a coastal section ~ 4km long which has a tripartite glacial sequence sitting over Permian Magnesian Limestone. The lower diamict is dark brown, crudely stratified in places, with shear and stringer structures composed of crushed Permian limestone common towards its base (Fig. 10). There are also occasional crude lenses of partially sorted gravel at the interface between underlying bedock and the diamict. Glacially abraded and striated clasts are common with a predominance of Permian Magnesian limestone, and Carboniferous limestones and sandstones. Overlying the lower diamict are up to 5m of well sorted sands and gravels that display much lateral variability with planar-bedded, rippled, channelised and foreset bedded sands. In places the sand are deformed, over-folded and contorted. They are overlain by a laterally discontinuous upper diamict which is dark brown in colour with frequent deformed intraclasts/pods of reworked sand. Glacially abraded and striated clasts are sparse. Three sand samples from the middle sands provided very consistent OSL ages ranging from 19.1 ± 1.9 (Shfd14065) – 19.9 ± 2.3 ka (Shfd14066; Table 2).

Geomorphology of the seafloor

Bedrock ridges

Major ridges are numbered R1 – R24 for ease of description and marked on both Figures 3b and 4a. R1 – 5 generally form a series of short ridges trending NE to SW in an area underlain by tilted and folded Cretaceous rock (Figs. 2a and 4a). R3 is a

discontinuous ridge that can be traced intermittently over 20-30 km and follows a faulted zone of Cretaceous and Jurassic rocks cutting through the Triassic rocks to the west. R2, 4 – 5 form much shorter ridges typically 5-10 km in length and only 1 - 3 m in amplitude. R6 is a sharp and well defined and coincides with an intrusive complex (Fig. 4a). R7 to R9 are less prominent and formed in Triassic rock. They are partially overlain by acoustic facies AF3 which forms a broad wedge (W1) in this region of the seafloor (Figs 3b, 4a, 4b). R10 has very little sediment cover and is cored by Permian rocks. R11 is a very prominent ridge. It is up to 8 - 10 m high, up to 20 km in length (though partially discontinuous), sharp crested in places with steep slopes and occasionally rectilinear in planform. R11 is on the boundary between the Triassic inlier and the Permian rock to the north. R12 is underlain by Permian bedrock and forms more of a prominent step in the seafloor topography. R13 coincides closely with the intrusion complex mapped closer to shore to the west (Figs. 2a, 4a). R14 - 18 are somewhat different in character to the ridges further south. They trend NE to SW but have rounded, low amplitude crests and form a corrugated pattern across the seafloor (Figs. 3a, 3b, 4a). They coincide with the boundary between the Permian strata and Carboniferous rocks further west (Fig. 2a). R19 - 24 are small, discontinuous, sharp-crested ridges formed in Carboniferous (Dinantian) strata, and which become draped in glaciogenic sediment to the north (Fig. 4a). It is clear from the acoustic and bathymetric data that large tracts of the seafloor are sediment deficient and floored by bedrock.

Sediment wedges and ridges

Two wedge-like features can be seen on the seafloor and are composed of sediment (W1 and W2; Figs. 3, 4). Wedge 1 (W1) is ~ 30 km wide and ~100 km in length. It runs NE to SW and is ~10 - 15 m high. It has an arcuate planform, an asymmetric geometry and convex upper surface with small surface perturbations where bedrock ridges are close to seafloor (e.g. R7 and R9; Fig. 4a). In cross-profile W1 displays a long, low angle dip slope to the north (proximal) and a steep, shorter southerly (distal) slope (Figs. 4a, 4b). It is composed of acoustic facies AF3, but also incorporates basal lenses of AF2 (up to 25m of sediment). Internal stratigraphic architecture was not discerned during cruise JC 123. Wedge 2 (W2) is smaller than W1, being ~9 - 12 m high, 3 to 5 km wide and ~25 km long (Figs. 3, 4a). It has an arcuate, wedge-like planform and a strong asymmetric geometry with a steep southerly slope (distal) and longer, gentler

northern slope (proximal). It is composed predominantly of acoustic facies AF3 with no apparent internal structure.

Unlike W1 and W2, the ridge marked M1 has a sinuous/multi-lobate planform that can traced over 25 km running NE to SW across northern part of the study area (Figs. 3, 4a). In cross profile it is symmetric and composed of glaciogenic sediment (AF3) that drapes Permian bedrock below. It has relatively gentle, low angle distal and proximal slopes with a distinctive central crest. There is perhaps a further section of M1 just north on R12 (Fig. 3b)

Lineations

Elongate and narrow lineations are common in the central part of the study area (Fig. 3). Most run northwest to southeast. They vary in planform; most are straight, but they can also be curved, sinuous and occasionally bifurcate. There is also a distinct sub-population that display an offset pattern with a northeast to southwest orientation (Fig. 3b). The length of the ridges spans from a few hundred meters up to ~10 km. Widths vary from tens to a few hundred meters, averaging 300 - 500m in width. Elongation ratios vary between 3:1 to 14:1. They rarely exceed 2 to 4 m in amplitude but this is dependent on sediment cover. Where Holocene sediment cover is sparse they have well defined steep slopes and rounded crests (Fig. 11a). Where sediment drapes are slightly thicker their surface form is more subdued (Figs. 11b, 11c). Many of the streamlined bedforms have a bedrock core forming the nucleus but there are examples where sediment (AF3) constitutes part of, or in rare cases, the whole bedform (Fig. 11c). In the west of the study area, data collected by the British Gelogical Survey in 1993/4, also shows streamlined bedforms buried beneath the seafloor. They are approximately 2–3 km long and 3–5 m in amplitude and appear to be constructed from AF3 (Fig. 11d).

When imaged at high resolution many of the bedforms appear to be seeded from perturbations on the seabed and are slightly tapered in that they are wider to the north and narrower to the south. It is also possible to see that some ridges are more ovate in planform (Fig. 12). Streamlined bedforms are sparse over W1. Indeed, they may be partially buried by W1 and it is clear from both the seafloor geomorphology (Fig. 3a) and

acoustic data (Fig. 4) that the bedrock surface in this area is buried by a significant sediment cover (AF3).

Channels

Several large channels can be seen in the northern half of the study area. Many of the depressions are narrow, elongate and have a low sinuosity. They are generally orientated NW - SE (Fig. 3). C1 is a broad flat channel that terminates close to R13. C2 is a well-defined single channel (Fig. 13a). C3 is a more complex system having a single channel north of M1, but appearing to split into C3 and C4 south of M1, before joining again and bending south-westwards. The main segments of C2 and C3 are over 20 km long. Their width varies between ~400 to ~2700 m wide. In cross-profile, they are mainly V-shaped and in long profile are irregular with undulatory long profiles (Fig. 13b; 13c). In places they are incised up to ~16 m deep into the seafloor. C5 is a more complex channel being formed of a series of partially disconnected segments and bends. There are also several small, highly sinuous channels superimposed on R11 (Fig. 12).

Interpretations and implications

The glacial imprint of the NSL offshore from the east coast has several distinctive elements. These include transverse bedrock ridges, subglacial channels, streamlined glacial lineations and till wedges. Together these form a mixed-bed glacial landsystem signature formed through glacial erosion (abrasion, streamlining and plucking), subglacial sediment deposition, subglacial meltwater excavation and, finally, deglacial glaciomarine sedimentation.

Bedrock influence on seafloor geomorphology

Transverse bedrock ridges trending NE to SW are prominent across the seafloor and formed in Carboniferous, Permian and Triassic rocks. In the north, the orientation of ridges R14 to R24 is controlled by the NE/SW axial orientation of synclines and anticlines in the Carboniferous strata (Fig. 14). R11-R13 also trend NE/SW but they lie within a zone of Permian strata with a Triassic inlier. They are not related to the large synclinal basin forming the Triassic inlier, but could be controlled either by faults or

regional igneous intrusions that run SW/NE from the coast towards the east (Fig. 14; e.g. Whin Sill). R7 to 10 are underlain by Permian and Triassic rocks but their relationship to the regional structural geology is unclear. However, R6 is clearly intrusive, lying close to the geological boundary between the Jurassic and Permian rocks (Figs. 4a,14). R1 – R5 trend NE to SW in an area underlain by tilted and folded Cretaceous rock (Fig. 4a), but R3 follows the fault bounded contact between the Cretaceous and Jurassic rock that trends westward (Fig. 14).

The bathymetric data suggest that the majority of bedrock ridges and surfaces in the study area are smoothed and abraded. There are occasional patches of bedrock that have 'rough' surfaces (e.g. see bedrock surfaces below core sites 133VC and 134VC; Fig. 6) but this is likely a product of the acoustic amplification of sub-vertical bedrock structure rather than a signal of plucking and quarrying. North of W1 the seafloor morphology is primarily controlled by the bedrock structure with secondary glacial streamlining of drift, which has resulted in a patchy subglacial mosaic of glaciogenic deposits and exposed bedrock (e.g. Eyles and Doughty, 2016; Fig. 3a). North of R12 bedrock close the seafloor and a thin drift cover has resulted in a relatively high bed roughness (Fig. 13).

The channels that run through the area north of R12 are clearly subglacial in origin as they have undulatory long profiles that signify water flowing under high pressure in Nye or tunnel channels (Fig. 13; e.g. Booth and Hallet, 1993; Ó Cofaigh, 1996; Clayton et al., 1999; Praeg, 2003). They perhaps formed when the ice margin was close to R12, and their NW to SE trajectory supports regional ice flow towards the southeast because subglacial water flow tends to broadly follow the regional ice sheet surface gradient (cf. Shreve, 1972; Booth and Hallet, 1993). The cutting of these channels into bedrock has further enhanced overall bed roughness/bumpiness of this area of the seabed in the area north of R12.

Subglacial sediment and landform genesis

The seismic data across the study area shows five distinct acoustic facies (Figs. 4, 5; AF 1-5). AF1 can be clearly identified as bedrock but AF2 and AF3 have characteristics similar to subglacial diamicts. AF2 is thin and patchy with variable thickness (~2 - 6 m). In contrast, AF3 forms distinctive, discontinuous sheets across the study area and has a

thickness ~4 and 10 m. It can thicken to 15–20m where it forms the wedges. Both AF2 and AF3 have high amplitude and highly irregular upper reflectors and are mainly acoustically transparent with little internal structure. AF3 occasionally has chaotic internal reflectors. MS measurements range from 100 to 629 x 10^{-5} SI probably due to differences in grain sizes and the concentration of magnetic minerals (Kilfeather et al., 2011; Hogan et al., 2016). Such acoustic properties have previously been interpreted as subglacial tills (Cameron et al., 1992; Gatliff et al., 1994; Huuse & Lykke-Anderson, 2000; Dove et al., 2017), with the heterogeneous nature of diamictic sediments resulting in acoustic homogeneity when observed in seismic profile (Hogan et al., 2016).

Cores 128VC, 133VC, 134VC and 135VC confirm this interpretation and all have diamictic sediments that were recovered from the top of AF3 (Fig. 6). From the core data, AF3 is predominantly massive, though occasionally partially stratified towards its upper contact. These diamicts are characterised by abundant clasts dispersed in a soft clay-silt matrix. Shear strength measurements for these facies range between ~11 - 70 kPa, which are lower values than reported for many subglacial tills (e.g. Boulton & Paul, 1976; Iverson et al., 1994; Clarke, 2005; Iverson, 2010), but similar shear strengths have been described from the West Antarctica continental shelf where soft subglacial diamicts are often associated with mega-scale glacial lineations (MSGL) (Dowdeswell et al., 2004; Ó Cofaigh et al., 2005 Evans et al., 2005; Kilfeather et al., 2011).

Foraminifera specimens were not found in all the diamictic units sampled, which also supports a subglacial origin, but the upward shift to partially stratified diamict in many of the cores suggests that these sediments are transitional from subglacial to proximal glaciomarine diamicts (e.g. Figs. 7a, 8a). The partially stratified and laminated silts and clays found within the upper parts of AF3 thus represent intermittent and gradual changes from subglacial deposition to processes dominated by undermelt, underflow/turbidity currents, ice rafted sediment, subaqueous debris flow and suspension settling (Gravenor et al., 1984; Hart and Roberts, 1994; Ó Cofaigh et al., 2005; Hogan et al., 2016). Possible low angle faults/shears in the diamict in 128VC (Fig 7a; section E/5) and minor disturbance and deformation of laminated units towards the top of AF3 (see Fig. 8a; core 135VC; section E/6) hint at minor lateral stress transfer through the sediment and subglacial/submarginal deformation of the sediment pile.

AF3 has been previously mapped as Wee Bankie Formation in the western NSB (Fig. 2b). It has been described as having a patchy distribution and being interspersed with bedrock exposures. Clast lithologies within it indicate a Scottish provenance (Cameron et al., 1992; Gatliff et al., 1994; Carr et al., 2006; Davies et al., 2011) and it is contiguous with the Bolders Bank Formation further south (Fig. 2b). Both formations therefore relate to the advance of the NSL, but due to the time-transgressive nature of glacier erosion and deposition (cf. Boulton 1996a, b), the Bolders Bank Formation is a 'down-ice' subglacial lithofacies produced via the net advection and thickening of subglacial till towards the southern margin of the NSL (Dove et al., 2017; Roberts et al., 2018), whereas the Wee Bankie Formation is a later subglacial lithofacies deposited as part of an active subglacial assemblage as the NSL retreated northwards.

Across the study area the AF3 facies is found in association with glacial lineations and sediment wedges, supporting a subglacial/sub-marginal origin (Clark, 1993; Stokes & Clark, 2001; Evans & Hiemstra, 2005). To the south of R11, the deepest areas of the seabed coincide with the synclinal Triassic inlier that runs south-southeast towards Newcastle (Fig.14). This area is heavily lineated and streamlined southwards towards W1 were the lineations dissipate and are perhaps buried beneath the wedge. Based on their shape and dimensions these bedforms are a mixture of drumlins and mega-scale glacial lineations (MSGL; Ely et al., 2016), and are a mix of hard and soft bed landforms. The elongate and narrow bedforms in the area between R11 and W1 vary in length from a few hundred meters up to ~10 km and in width from tens to a few hundred meters (~ 300 - 500m). Amplitudes are ~ 2 - 4 m and their elongation ratios vary between 3:1 and 14:1. They are analogous to MSGL mapped in other formerly glaciated regions (e.g Clark 1993, 1994; Stokes and Clark 2002; Spagnolo et al., 2014; Ely et al., 2017). Figure 11a displays the cross profile form of the MSGL on the seafloor but it is difficult to be certain whether they are bedrock or till cored. To the immediate east of R10 and R11 the MSGL appear to closely coincide with the axial orientation of multiple small scale synclines and anticlines mapped within the Triassic sequence associated with the Farne Deeps (Fig.14). In other areas, the MSGL appear to bifurcate and anastomose. The sub-population marked in orange in Figure 3b exhibit an offset pattern (northeast to southwest orientation) which perhaps relates to bedrock influence sub-parallel to the main synclinal axis of the Triassic inlier (Fig.14). Other lineations (marked as minor bedrock ridges; Fig. 3b) are very sinuous suggesting bedrock influence. There is also the possibility some could be eskers but this requires further investigation.

There are clear bedrock cores in streamlined bedforms to the immediate south of R11 (Fig. 11c). These bedforms are slightly more ovate and drumlinoid in planform (Fig. 3a) but they have bedrock cores with glaciogenic material mainly concentrated in the lows between bedforms. The MSGL south of 132VC display a thin veneer of glaciogenic material (AF3) over bedrock bumps in the north but, as drift thickness increases southward (Fig. 4b) the upper surface of AF3 becomes streamlined (drumlinised) and the influence of bedrock perturbations is reduced. Slightly further west, seismic records acquired by the BGS (1993-1-1) also possibly show buried streamlined drumlins, though have previously been interpreted as subaqueous dunes formed by tidal currents (Brew, 1996; a theory somewhat incompatible with ice sheet retreat under glaciomarine conditions; see below) (Fig. 11d). However, to the immediate east of core 134VC bedrock again forms the core of large, moulded, bedrock hills on the seafloor (Figs. 3a, 4b). Hence, it is a combination of sediment distribution and thickness, plus bedrock roughness, that controls bedform-type and position in relation to regional ice flow, as well as determining the patchiness of the glaciogenic sediment cover in this upstream part of the NSL.

When imaged using high-resolution bathymetry many of the MSGL have seed points, suggesting that bedrock knobs are close to the surface and trigger bedform initiation, with pervasive deposition and deformation subglacial till being contemporaneous with the evolution of the MSGL's (cf. Boulton, 1971, 1975, 1982, 1987; Jansson and Kleman 1999; Stokes et al. 2013; Spagnolo et al., 2016). North of R12 there only are a few MSGL, suggesting thin sediment cover over the bedrock, however, the MSGL are better developed where sediment is thickest between R12 and R11 and south of R11 (see Fig. 4a between R10-R13 and Fig. 12). The complete lack of MSGL over R11 (see Fig. 12) shows there is little subglacial sediment over this ridge. The juxtaposition of both bedrock-cored and sediment-cored bedforms also reinforces the notion that in areas of thin drift cover the subglacial bed is partially emergent and partially inherited, with bedform assemblages both evolving and hybridised via a combination of erosion, deposition and deformation (Clark et al., 2010; 2018; Eyles et al., 2016). Many of the MSGL in the central study area (Fig. 12) are pinned to bedrock bumps or initiator scarps and, thus, their position and distribution is a function of both bedrock morphology and sediment supply.

W1 and W2 (Figs. 3 and 4) are clearly grounding zone wedges (GZW) (Powell 1990, 2003; Ottesen & Dowdeswell, 2006; Batchelor and Dowdeswell, 2015). They are asymmetric sedimentary depo-centres with distinctive wedge geometries, associated with the accretion of subglacial material at the grounding line of the NSL as it has receded northwards (Figs. 15; 16). From the acoustic data in can be seen that both W1 and W2 are composed of AF2 and AF3 but they lack clear internal structure. Neither is well streamlined, but the association of MSGL positioned upstream of W1 suggests that the net flux of subglacial material via bed deformation and MSGL formation was critical to the construction of a large GZW (Anderson and Bartek, 1992; Powell and Domack, 1995; O Cofaigh et al., 2005; Ottesen et al., 2007; Batchelor & Dowdeswell, 2015).

Dove et al. (2017) have recently demonstrated that the NSL underwent a series of quasi-stable oscillations during recession, depositing a series of superimposed, lobate-shaped till wedges offshore from Norfolk and Yorkshire. This pattern of repeated oscillation, till sheet deposition and incremental thickening has been mapped also onshore along the Yorkshire coast by Boston et al. (2010) and Evans & Thomson (2010), but the exact mechanisms and timing of emplacement of W1 and W2 are more difficult to discern. W2 is constructed exclusively of AF3 with no discernible internal architecture. W1 has discontinuous lenses of AF2 overlain by AF3, suggesting the emplacement of one till sheet over the other. This suggests that the ice margin was stable and receiving a net surplus of subglacial material for some time, but it is difficult to establish the exact processes that formed W1 and W2 without more detailed acoustic stratigraphy. W1 is much larger than W2, which could imply a more prolonged still-stand, but without an improved knowledge of sediment flux rates, or a better constrained chronology, this cannot be substantiated.

There is evidence for an additional still-stand/re-advance event as ice retreated north of W1 in the form of M1, which has a very different planform to W1 and W2. Its multi-lobate nature is more similar to a terminal/push moraine complex (Fig. 3; e.g. Dredge and Cowan 1989; Patterson 1997, 1998; Colgan 1999; Evans et al. 2008, 2014; Colgan et al. 2003; Kovanen and Slaymaker 2004). This may simply represent a shorter-lived event than those that constructed W1 and W2, and thus the distinctive imprint of a lobate ice margin has been preserved on the seafloor and not been obscured by the continual net advection of sediment to the ice margin (to form a more substantive till sheet/wedge).

Temporary standstill of the ice margin in order to form the GZW's may have been both internally and externally controlled. Changes in bed configuration (there are multiple bedrock highs forming pinning points below W1; Figs. 4 and 15) or water depth at the margin (e.g. as sea-level increased) are two probable mechanisms that influenced grounding line stability (Powell and Alley, 1987; Schoof, 2007). Changes to ice dispersal centres and shifting ice divides over Scotland and the northern North Sea would also have been important in determining the flow behaviour of ice flowing offshore through the Firth of Forth and into the NSL during regional deglaciation. What is clear from the imprint of W1, M1 and W2 is that the NSL was behaving as a piedmont lobe flowing NW to SE during overall northwards recession. The glacial imprint offshore of County Durham and Northumberland does not support the action of a defined ice stream trunk zone (with lateral shear margins; Stokes and Clark, 2001; Golledge and Stoker, 2006), nor does it provide any evidence for the eastward extensions of the Tweed or Tyne Gap Ice streams during the early phases of the LGM (Davies et al., 2009; Livingstone et al., 2015).

The NSL therefore, does not exhibit the classic features associated with ice stream onset zones such as convergent flow patterns, distinct lateral shear margins or a trunk zone (Stokes and Clark, 2001), however, it does share some the hard/mixed, streamlined bed characteristics described from other former ice onset zones sourced from upland Britain (e.g. Minch Ice Stream and Hebridean Ice Stream; Bradwell et al. 2007, 2013, 2015; Dove et al., 2015; Krabbendam et al, 2016) and Scandanavia (Ottesen et al,. 2016). The onset zone of the Minch Ice Stream in particular, where both soft-bed and hard-bed subglacial landform assemblages in the central and inner parts of the Minch mark grounded fast-flowing ice and a high degree of ice-bed coupling is very similar to the glacial landsystem reported herein. The transition from scoured and streamlined bedrock terrain to MSGL has also been used to infer an increase in ice flow velocity as ice passes from a hard to a soft bedded substrates in other ice stream onset settings such as the Hebridean Ice Stream and Norwegian Channel ice Stream (Dove et al., 2015; Ottesen et al,. 2016). In our study area, MSGL do occur in a specific zone south of the bedrock dominated terrain between R11 – 18 and north of W1 (Fig 3b) possibly reflecting a period ice streaming to an ice margin at W1.

Upstream of the study area direct evidence for ice stream onset within the Firth of Forth has been established by Golledge et al. (2006) who demonstrated the areas to the north of the Firth of Forth formed the Strathmore Ice Stream flowing northeastward. In addition, other recent work along the southern shore of the Firth of Forth also indicates preferential westerly ice flow directly feeding the NSL (Hutton, 2018). On balance therefore, it seems logical that the mixed-bed subglacial landsystem and GZW's identified beneath the NSL are clear evidence of an ice stream lobe operating along the southern edge of the Firth of Forth and undergoing transition from a terrestrial piedmont-lobe margin with a net surplus of sediment to the south (Dove et al. 2017), to a dynamic, quasi-stable, tidewater margin as the ice withdrew into the Firth of Forth (Fig. 16).

The combined influence of enhanced flow velocities and grounding line instability triggered by marine inundation of the central North Sea would have been critical mechanisms controlling the development of the mixed-bed signal during deglaciation. Bed excavation in places down to bedrock, increasing bed roughness, till advection and GZW construction were likely all key feedbacks influencing the landsystem signature. In themselves, the GZW's observed in this study are unusual in that they are not associated with a cross-shelf trough or major fjord system. Instead they chart the retreat of a regional scale, collapsing, marine-based lobate ice stream margin (cf. Patterson 1997; Jennings 2006).

Deglaciation: Glaciomarine deposition

AF4 was sampled in all the cores in the study area. It is characterised by fine-grained, interlaminated sediments. Microscale ripples, and planar cross lamination in some cores indicates underflow activity in a proximal setting close to a grounding line (Fig. 9a; Core 136VC; Smith and Ashley 1985; Kneller and Buckee 2000; Mulder and Alexander 2001). The laminated clays and silts are a product of suspension settling with coarser silt and fine sand laminae representing rainout from proximal meltwater plumes (Powell 2000, 2003). The frequency of switches in grain size signify an environment dominated by episodic meltwater input. In core 135VC, increasingly distal conditions are marked up-core by a decrease in the frequency of laminae and an increase in the thickness of clay laminae (Fig. 8a). This is replicated in cores 134VC and 128VC. The abundance of cold water foraminifera species also suggests these are glaciomarine sediments.

Elphidium excavatum (clavatum) and *Cassidulina reniforme* are known indicators of extreme glacial marine environments, and other indicator species such as *Elphidium incertum, Elphidium asklundi*, *Elphidium albiumbilicatum, Haynesina orbiculare* and *Bolivina sp*. further corroborate cold glaciomarine conditions (Feyling-Hanssen, 1972; McCabe et al., 1986; Hansen & Knudsen, 1995; Lloyd et al., 2005; Peters et al., 2015)

In cores 132 and 136VC the lower laminated sequences are overlain by diamictic units (Figs. 7b and 9a). This could suggest ice marginal re-advance and the deposition of subglacial till. In 136VC this possibly relates to the margin stabilising on the high ground/pinning points provided by R1-R5 (Figs. 3b, 4a). Alternatively, the diamict in 136VC could be a glaciogenic debris flow or mud apron, because two distinctive off-lapping sheets of sediment thicken downslope (north to south) to the basin floor (see core site 136VC in Figs 4a, 6; c.f. Kristensen et al. 2009; Carto and Eyles 2012; Talling 2014). Contrary to this, 135VC just to the north of 136VC shows an increasingly distal record, suggesting it has not been influenced by any local ice marginal re-advances. Core 132VC also contains a diamict sandwiched between two laminated units, indicating a possible later re-advance as ice migrated northward towards M1 and W2. Dropstones in many of the laminated units indicate deposition of ice rafted debris (Thomas and Connell 1985; Gilbert 1990; Hart and Roberts, 1994, Ó Cofaigh & Dowdeswell, 2001), although it is noteworthy in 135VC, 136VC and 137VC (Figs. 8a, 9) that the interlaminated facies often lack clasts, possibly inferring sub-ice shelf conditions during retreat (Drewry and Cooper 1981; Ó Cofaigh et al. 2001), but this requires further investigation.

These sediments have previously been mapped as the Forth, St Abbs and Sunderland Ground Formations across the study area (Fig 2b; Cameron et al., 1992; Gatliff et al., 1994). From the acoustic data collected as part of this project (Fig. 4) they are clearly restricted to small, local basins/depo-centres and as such represent time transgressively deposited pockets of glaciomarine sediment as the NSL receded northwards (Fig. 15). A regional signal of increasingly distal conditions is not discernible as each local depo-centre is a repeat package and produced by an active, receding margin (cf. Thomas et al., 2004). AF4 therefore represents a change from proximal to distal conditions through time, and the rhythmicity of the interlaminated sediments is primarily a product of grounding line proximity and changing meltwater flux. The Nye channels mapped north of R12 provide evidence for subglacial meltwater flux to the

grounding line, but they are not ubiquitous across the region, hence supraglacial melt could also have been important in influencing water column stratification and mixing (Smith and Ashley 1985; Cowan and Powell 1990; Powell 1990, 2003). AF5 is interpreted as Holocene and contemporary seafloor sediments with gravel lags, poorly sorted sands and shell hash indicative of current reworking across the seafloor (Balson et al., 2001).

Discussion: the timing and forcing of regional deglaciation

Recent OSL ages from the southern North Sea place the NSL on the Norfolk coast after 22.8 – 21.5 ka (Roberts et al., 2018). That final phase of NSL advance to the south was followed by ice recession and Dove et al. (2017) chart a series of large arcuate, lobate moraines formed as the NSL margin migrated north, parallel with the Lincolnshire and Yorkshire coasts (Fig. 17). As the ice retreated northwards, Bateman et al. (2017) constrain final deglaciation of East Yorkshire coast to >17 ka based on OSL ages relating to the final stages of Glacial Lake Humber at Hemingborough and Ferrybridge and post-glacial sediments found at Barmston, Sewerby and Heslerton (Fig. 17). Slightly further north in the Vale of Pickering, Evans et al. (2017) suggest the NSL thinned and receded offshore from the Yorkshire coast at ~ 17.6 ka based on ages from Heslerton. Further north again, cosmogenic dates from Tyne Gap show ice had withdrawn westward from the coast by 17. 8 to 17.6 ka, although geomorphic evidence indicates that the NSL occupied the coast until slightly later (Livingstone et al., 2015).

The new radiocarbon dates for cores 132VC and 137VC signify deglaciation of the NSL offshore prior to 19.9 - 19.5 ka cal. BP. These dates are supported by new OSL dates on glacial outwash from Seaham on the Durham coast which suggest final deglaciation after ~ 19.6 ka, as the western margin of the NSL migrated north (Table 2). These dates are somewhat earlier (although within errors) than OSL dates from the Yorkshire region (Bateman et al. 2017; Evans et al. 2017), and also out of phase with the cosmogenic dates from the Tyne Gap west of Newcastle (Livingstone et al., 2015). Given the lateral extent and geometry of W1, as well as the regional footprint of the NSL, it seems unlikely that the lobate termini of the NSL would differentially retreat along its central axis, because it was sourced and controlled by ice from the Firth of Forth in its latter stages. Therefore further dating control between Lincolnshire, Yorkshire, Durham and

Northumberland is required to reconcile NSL recession rates as it pulled back from its maximal extent in Norfolk to the Firth of Forth.

Foraminifera from the distal glaciomarine sediments lying above subglacial till in core 128VC (AF3; Fig 4a; Table 1) signify deglaciation prior to 16.9 ka cal. BP (Fig. 17). This age is further supported by onshore dates from the Tay and Forth estuaries where glaciomarine sediments associated with the Errol Beds Formation show ice had moved west of the present coastline by 16.9 to 16.0 ka cal BP (Fig 17; Table 3; Hedges et al. 1989; Peacock & Browne 1998; Peacock 2002; see Hughes et al., 2011 for overview). An additional Britice-Chrono core (118VC; Fig. 17) contains distal glaciomarine sediments lying over subglacial till dated to 17.8 to 16.5 ka cal. BP (Table 1), and corroborates the general pattern and rate of ice retreat into the Firth of Forth; though it should be noted that this site lies slightly north of the main flow trajectory of the NSL and, as such, glacier/ice stream dynamics in this region of the Firth of Forth may have been slightly different during deglaciation.

Defining the mechanisms that controlled deglaciation of the NSL between 20 ka and 16ka is challenging. It is clear from the acoustic stratigraphy and core data that the NSL retreated under glaciomarine conditions. The northern and central NSB was inundated during this period and, although sea-level reconstructions predict that pre 12ka sea-level was either static (16-20ka) or falling (16-12ka) (Bradley et al., 2011), instantaneous inundation would have triggered a grounding line response. The GZW's identified as part of this study (W1 and W2) indicate quasi-stable conditions during overall recession. W1 in particular points to a prolonged period of ice margin stability prior to 17ka. This is also a period when ice feeding through the Firth of Forth would have experienced significant changes in ice flux, with shifting ice divides over central Scotland. Such changes were a response firstly to decoupling of the FIS and BIIS (Sejrup et al., 2015; Merritt et al., 2017), followed by air temperature and insolation driven thinning (Alley and Clark., 1999; Bintanja et al., 2005), as well as possible mass balance and dynamic feedbacks relating to westerly sectors of the BIIS responding to the Heinrich 1 cooling (McCabe et al., 1998).

The mixed-bed footprint of the NSL offshore from Durham and Northumberland was therefore a product of several key processes and feedbacks operating during deglaciation, all of which contributed to rapidly change basal, supraglacial and ice

marginal conditions. Marginal instability and drawdown of the NSL were controlled primarily by upstream shifts in ice divide position and regional ice stream flux via the Firth of Forth. Water depths and ice thickness would also have been instrumental in promoting instability at the grounding line. Together with rates of ice surface thinning and meltwater production (increased insolation and air temperatures) these would have been instrumental in lubricating the bed and promoting ice streaming, bed decoupling/basal sliding, bedrock abrasion, till advection, MSGL formation and ultimately GZW formation. It is the production of the GZW's in particular that points to a dynamic subglacial system able to excavate its bed and advect till to a grounding line in order to stabilise the NSL during overall retreat. This infers a very unstable glaciological regime in the latter phases of MIS 2 glaciation with a complex set of both internal and external driving mechanisms producing a distinctive mixed-bed subglacial landsystem beneath a retreating, marine-terminating, ice stream lobe in the western North Sea.

Conclusions

New geophysical data, sediment cores and radiocarbon dates from the western North Sea provide fresh insights into the signature and behaviour of the North Sea Lobe during the closing stages of the LGM. Four acoustic facies can be mapped across the study area and interpretations supported using sediments cores. Subglacial tills (AF2 and AF3) form a discontinuous and patchy mosaic of glaciogenic sediments often interspersed with bedrock outcrops and ridges. This mosaic forms a 'mixed-bed' landsystem with bedrock structure and glacial erosion (abrasion and plucking) controlling the position and form of large transverse ridges, but with partial excavation and the net advection of subglacial sediment producing MSGL and GZW's. On a regional scale, this mixed-bed signal of the NSL represents a dynamic switch from a terrestrial streaming piedmont-lobe margin with a net surplus of sediment to the south (Dove et al. 2017), to a partially erosive/excavational, quasi-stable, marine-terminating, ice stream lobe as the ice withdrew northwards.

Glaciomarine sediments are distributed in local depo-centres and basins across the study area and drape the underlying subglacial mixed-bed imprint. The proximal deposition of material was dominated by meltwater plumes, producing thick interlaminated sequences of sands, silts and clays, with secondary inputs from glaciogenic debris flows and underflows. More distal glaciomarine facies are

characterised by silts and clays deposited from suspension with additional IRD inputs. Foraminifera assemblages are domainated by *Elphidium clavatum* which is a known indicator of extreme glacial marine environments, and several other species corroborate cold glaciomarine conditions.

In the area offshore from the Durham and Northumberland coasts, new radiocarbon dates suggest that the NSL retreated under tidewater conditions between 19.9 ka and 16.5ka. This is somewhat earlier than OSL and cosmogenic ages from the Yorkshire coast and Tyne Gap area, but these new ages can be reconciled with deglacial dates from the Tay and Forth estuaries indicative of ice retreat at ~ 16.9 to 16.0 ka cal. BP. The dominant controls on the rates of ice recession and groundling line stability during this period were ice flux through the Firth of Forth Ice stream onset zone and water depths at the grounding line, perhaps supplemented by accelerating rates of ice surface thinning and meltwater flux as the climate warmed. However, secondary feedbacks relating to hard to soft bed transition, with bed excavation to partial bedrock, increasing bed roughness, till advection and GZW construction were also key factors influencing the distinctive mixed-bed imprint of a marine-terminating, ice stream lobe in the western North Sea.

Acknowledgements

This work was supported by the EU ITN *Glaciated North Atlantic Margins* (GLANAM) project and Natural Environment Research Council consortium grant*; BRITICE-CHRONO* NE/J009768/1. Data was collected during cruise JC123 in summer 2015. The authors would like to extend their thanks the crew of the RRs James Cook and the BGS and Britice-Chrono science teams who supported the planning and execution of this work. HAS and DD publish with permission of the Executive Director of the British Geological Survey. Multibeam echosounder data shown in Fig 4E were collected as part of the ‘Coordination of the Defra Marine Conservation Zone data collection programme 2011/12’ funded by the Department of Environment, Food and Rural Affairs of the United Kingdom. The radiocarbon analyses were supported by the NERC Radiocarbon Facility NRCF010001 (allocation number 1976.1015.013). Chris Orton of the Design and Imaging Unit at Durham University is thanked for his help with several figures.

References

Alley R, Clark PU. 1999. The deglaciation of the northern hemisphere: A global perspective. *Annual Review of Earth and Planetary Sciences* 27: 149-182

Anderson JB, Bartek LR. 1992. Ross Sea glacial history revealed by high resolution seismic reflection data combined with drill site information. In The Antarctic Paleoenvironment: A

Perspective on Global Change, Kennett JP, Warnke DE. (eds). 1. Antarctic ResearchSeries 56. American Geophysical Union, Washington, DC, 231–263.
Balson P, Butcher A, Holmes R, Johnson H, Lewis M, Musson R. 2001. North Sea Geology. BGS SEA2 Technical report.
Balson PS, Jeffrey DH. 1991. The glacial sequence of the southern North Sea. In Glacial Deposits of Great Britain and Ireland, Ehlers J, Gibbard PL, Rose J. (eds): Balkema, Rotterdam, 245–254.
Batchelor CL, Dowdeswell JA. 2015. Ice-sheet grounding-zone wedges (GZWs) on high-latitude continental margins. *Marine Geology* 363: 65–92.
Bateman MD, Catt JA. 1996. An absolute chronology for the raised beach deposits at Sewerby, E. Yorkshire, UK. *Journal of Quaternary Science* 11: 389-395.
Bateman MD., Buckland P C, Chase B, Frederick CD, Gaunt GD. 2008. The Late-Devensian proglacial Lake Humber: new evidence from littoral deposits at Ferrybridge, Yorkshire, England. *Boreas* 37: 195–210.
Bateman M D, Buckland PC, Whyte MA, Ashurst RA, Boulter C, Panagiotakopulu E. 2011. Re-evaluation of the Last Glacial Maximum typesite at Dimlington, UK. *Boreas* 40: 573–584.
Bateman MD, Evans DJA, Buckland PC, Connell ER, Friend RJ, Hartmann D, Moxon H, Fairburn WA, Panagiotakopulu E, Ashurst, RA. 2015. Last Glacial dynamics of the Vale of York and North Sea Lobes of the British and Irish Ice Sheet. *Proceedings of the Geologist's Association 126*: 712-730.
Bateman MD, Evans, DJA, Roberts DH, Medialdea A, Ely J, Clark CD. 2017. The timing and consequences of the blockage of the Humber Gap by the last British- Irish Ice Sheet. *Boreas* 47: 41-61.
Bintanja R, van de Wal RS, Oerlemans J. 2005. Modelled atmospheric temperatures and global sea levels over the past million years. *Nature* 437: 125-128.
Bisat WS. 1932. On the sub-division of the Holderness boulder clays. *The Naturalist Hull:* 215 – 219.
Booth DB; Hallet B. 1993. Channel networks carved by subglacial water - Observations and reconstruction in the eastern Puget Lowland of Washington, U.S.A. *Geological Society of America* 105: 671 -683.
Boston CM, Evans DJA, Ó Cofaigh C. 2010. Styles of till deposition at the margin of the Last Glacial Maximum North Sea lobe of the British-Irish Ice Sheet: an assessment based on geochemical properties of glacigenic deposits in eastern England. *Quaternary Science Reviews* 29: 3184–3211.
Boulton GS. 1976. The origin of glacially fluted surfaces: observations and theory. *Journal of Glaciology* 17: 287–309.
Boulton GS, Paul MA (1976) The influence of genetic processes on some geotechnical properties of tills. *Journal of Engineering Geology* 9: 159–194.
Boulton GS. 1987. A theory of drumlin formation by subglacial sediment deformation. In Drumlin symposium, Menzies J; Rose J. (eds): A. A. Balkema [Rotterdam], 25-80.
Boulton GS, Jones AS, Clayton KM,Kenning MJ. 1977. A British ice sheet model and patterns of glacial erosion and deposition in Britain. In British Quaternary Studies, Shotton FW. (ed): Oxford University Press, 231-46
Boulton GS, Smith GD, Jones AS, Newsome J. 1985. Glacial geology and glaciology of the last mid-latitude ice sheets. *Journal of the Geological Society of London*142: 447-474.
Boulton GS. 1971. Till genesis and fabric in Svalbard, Spitsbergen. In Till – A Symposium, Goldthwait RP (ed): Ohio State University Press, 41-72.
Boulton GS. 1975. Processes and patterns of subglacial drainage: A theoretical approach. In Ice Ages: Ancient and Modern, Wright AE, Moseley F, (eds): Seal House, Liverpool, 7-42
Boulton GS. 1982. Subglacial processes and the development of glacial bedforms. In Research in Glacial, Glacio-fluvial and Glaciolacustrine Systems, Davidson-Arnott R, Nickling W, Fahey BD. (eds.): Geo Books, Norwich, 1–31.
Boulton GS. 1990. Sedimentary and sea level changes during glacial cycles and their control on glacimarine facies architecture. *Geological Society, London, Special Publications* 53: 15–52.
Boulton GS. 1996a. The origin of till sequences by subglacial sediment deformation beneath mid-latitude ice sheets. *Annals of Glaciology* 22: 75–84.
Boulton GS. 1996b. Theory of glacial erosion, transport and deposition as a consequence of subglacial sediment deformation. *Journal of Glaciology* 42: 43–62.

Boulton GS, Hagdorn M. 2006. Glaciology of the British Isles Ice Sheet during the last glacial cycle: form, flow, streams and lobes. *Quaternary Science Reviews* 25: 3359–3390.
Bradley SL, Milne GA, Shennan I, Edwards R. 2011. An improved glacial isostaticadjustment model for the British Isles. *Journal of Quaternary Science* 26: 541–552.
Bradwell, T., 2013. Identifying palaeo-ice-stream tributaries on hard beds: mapping glacial bedforms and erosion zones in NW Scotland. Geomorphology 201, 397–414.
Bradwell, T., Stoker, M.S., 2015. Submarine sediment and landform record of a palaeo-ice stream within the British−Irish Ice Sheet. Boreas 44, 255–276.
Bradwell, T., Stoker,M.S., Larter, R., 2007. Geomorphological signature and flow dynamics of The Minch palaeo-ice stream, northwest Scotland. Journal of Quaternary Science 22, 609–617.
Brew DS. 1996. Late Weichselian to early Holocene subaqueous dune formation and burial off the North Sea Northumberland coast. *Marine Geology* 134: 203-211.
Bronk Ramsey C. 2009. Bayesian analysis of radiocarbon dates. *Radiocarbon* 51: 337-360.
Cameron TDJ, Crosby A, Balson PS, Jeffrey DH, Lott G., Bulat J, Harrison DJ. 1992. United Kingdom offshore regional report: the geology of the southern North Sea.London: HMSO for the British Geological Survey.
Carr SJ, Holmes R, Van Der Meer JJ, Rose J. 2006. The Last Glacial Maximum in the North Sea Basin: micromorphological evidence of extensive glaciation. *Journal of Quaternary Science* 21: 131–153.
Carto SL, Eyles, N. 2012. Sedimentology of the Neoproterozoic (c. 580 Ma) Squantum 'Tillite', Boston Basin, USA: Mass flow deposition in a deep-water arc basin lacking direct glacial influence. *Sedimentary Geology*, 269, 1–14.
Catt JA. 2007. The Pleistocene glaciations of eastern Yorkshire: a review. *Proceedings of the Yorkshire Geological Society* 56: 177–207.
Clark CD, Tulaczyk, SM, Stokes CR, Canals M. 2003. A groove-ploughing theory for the production of mega-scale glacial lineations, and implications for ice-stream mechanics. *Journal of Glaciology* 49: 240–256.
Clark CD, Ely, Jeremy C, Spagnolo M, Hahn U, Hughes Anna C, Stokes CR. 2018. Spatial organization of drumlins. *Earth Surface Processes and Landforms* 43: 499-513
Clarke GKC. 2005. Subglacial processes. *Annual Review Earth Planet Science letters* 33: 247–276.
Clayton L, Atti, JW, Mickelson DM. 1999. Tunnel channels formed in Wisconsin during the last glaciation. In Glacial Processes Past and Present, Mickelson DM, Attig JW. (eds.): Geological Society of America, Special Paper 337, 69–82.
Colgan PM. 1999. Reconstruction of the Green Bay Lobe, Wisconsin, United States, from 26,000 to 13,000 radiocarbon years. In Glacial Processes Past and Present, Mickelson DM. Attig JW. (eds.): Geological Society of America Special Paper 337, Boulder, Colorado, 137–150.
Colgan PM, Mickelson DM, Cutler PM. 2003. Ice marginal terrestrial landsystems: southern Laurentide ice sheet margin. In Glacial landsystems, Evans D.J.A (ed): Arnold, London, 111-142.
Cotterill CJ, Phillips E, James L, Forsberg CF, Tjelta, TI, Carter, G, Dove D. 2017. The evolution of the Dogger Bank, North Sea: A complex history of terrestrial, glacial and marine environmental change. *Quaternary Science Reviews* 171: 136–153.
Cowan EA, Powell RD. 1990. Suspended sediment transport and deposition of cyclically interlaminated sediment in a temperate glacial fjord, Alaska, USA. *Geological Society, London, Special* Publications 53: 75–89.
Cowan EA, Seramur KC, Cai J, Powell RD. 1999. Cyclic sedimentation produced by fluctuations in meltwater discharge, tides and marine productivity in an Alaskan fjord. *Sedimentology* 46: 1109–1126.
Davies BJ, Roberts DH, ÓCofaigh C, Bridgland DR, Riding J., Philipps, ER, Teasdale DA. 2009. Interlobate ice-sheet dynamics during the Last Glacial Maximum at Whitburn Bay, County Durham, England. *Boreas* 38: 555–578.
Davies BJ, Roberts, DH, Bridgland, DR, Ó Cofaigh C, Riding JB. 2011. Provenance and depositional environments of Quaternary sediments from the western NorthS ea Basin. *Journal of Quaternary Science* 26: 59–75.

Davies BJ, Roberts DH, Bridgland DR, Ó Cofaigh C. 2012a. Dynamic Devensian ice flow in NE England: a sedimentological reconstruction. *Boreas* 41: 337–336.

Davies BJ, Roberts DH, Bridgland DR, Ó Cofaigh, C, Riding JB, Demarchi B,Penkman, KEH, Pawley, SM. 2012b. Timing and depositional environments of a Middle Pleistocene glaciation of northeast England: New evidence from Warren House Gill, County Durham. *Quaternary Science Reviews* 44: 180–212.

Dove D, Arosio R, Finlayson A, Bradwell T, Howe JA. .2015. Submarine glacial landforms record Late Pleistocene ice-sheet dynamics, Inner Hebrides, Scotland. *Quaternary Science Reviews* 123: 76–90.

Dove D, Evans DJA., Lee JR, Roberts DH, Tappin DR, Mellett CL, Long D, Callard SL 2017. Phased occupation and retreat of the last British–Irish Ice Sheet in the southern North Sea; geomorphic and seismostratigraphic evidence of a dynamic ice lobe. *Quaternary Science Reviews* 163: 114–134.

Dowdeswell, JA, Fugelli EMG. 2012. The seismic architecture and geometry of grounding-zone wedges formed at the marine margins of past ice sheets. *Geological Society of America Bulletin 124*: 1750–1761.

Dowdeswell, JA, ÓCofaigh C, Pudsey CJ. 2004. Thickness and extent of the subglacial till layer beneath an Antarctic paleo–ice stream. *Geology* 32: 13–16.

Dredge LA, Cowan WR. 1989. Quaternary geology of the southwestern Canadian Shield. In Quaternary Geology of Canada and Greenland, Fulton RT. (ed): Geological Survey of Canada, 214-235.

Drewry DJ, Cooper APR. 1981. Processes and models of Antarctic glaciomarine sedimentation. *Annals of Glaciology* 2: 117-122.

Ely JC, Clark CD, Spagnolo M, Hughes ALC, Stokes CR. 2018. Using the size and position of drumlins to understand how they grow, interact and evolve. *Earth Surface Processes and Landforms* 43: 1073-1087

.Evans DJA, Clark CD, Rea BR. 2008. Landform and sediment imprints of fast glacier flow in the southwest Laurentide Ice Sheet. *Journal of Quaternary Science* 23: 249-272

Evans DJA, Benn D. 2004. A practical guide to the study of glacial sediments. Arnold, London.

Evans DJA, Benn, DI. 2004. Facies description and the logging of sedimentary exposures. In A Practical Guide to the Study of Glacial Sediments, Evans, DJA Benn, DI (eds): Arnold, London, 11-51.

Evans D JA, Hiemstra JF. 2005. Till deposition by glacier submarginal, incremental thickening. *Earth Surface Processes and Landforms* 30: 1633–1662.

Evans DJA, Thomson SA. 2010. Glacial sediments and landforms of Holderness, eastern England: a glacial depositional model for the North Sea Lobe of the British–Irish Ice Sheet. *Earth Science Reviews* 101: 147–189.

Evans DJA, Owen LA, Roberts DH. 1995. Stratigraphy and sedimentology of Devensian (Dimlington-Stadial) glacial deposits, East Yorkshire, England. *Journal of Quaternary* Science 10: 241-265.

Evans DJA, Clark CD, Mitchell WA. 2005. The last British Ice Sheet: A review of the evidence utilised in the compilation of the Glacial Map of Britain. *Earth-Science Reviews* 70: 253–312.

Evans, DJA., Hiemstra JF, Boston C., Leighton I, Ó Cofaigh C, Rea, BR. 2012. Till stratigraphy and sedimentology at the margins of terrestrially terminating ice streams: case study of the western Canadian prairies and high plains. Quaternary Science Reviews 46, 80–125.

Evans DJA., Young NJP, Ó Cofaigh C. 2014. Glacial geomorphology of terrestrial- terminating fast flow lobes/ice stream margins in the southwest Laurentide Ice Sheet. *Geomorphology* 204: 86-113.

Evans DJA., Bateman, MD, Roberts, DH, Medialdea, A, Hayes L, Duller GAT, Fabel D, Clark CD. 2017. Glacial Lake Pickering: stratigraphy and chronology of a proglacial lake dammed by the North Sea Lobe of the British–Irish Ice Sheet. Journal of Quaternary Science 32: 295–310.

Everest J, Bradwell T, Golledge N. 2005. Subglacial landforms of the Tweed Palaeo-Ice stream. *The Scottish Geographical Magazine* 121: 163–173.

Eyles N, Sladen JA, Gilroy S. 1982. A depositional model for stratigraphic complexes and facies superimposition in lodgement tills. *Boreas* 11: 317-33.

Eyles N. 2012. Rock drumlins and megaflutes of the Niagara Escarpment, Ontario, Canada: a hard bed landform assemblage cut by the Saginaw–Huron Ice Stream. *Quaternary Science Reviews* 5: 34–49.
Eyles N, Doughty M. 2016. Glacially-streamlined hard and soft beds of the paleo-Ontario ice stream in Southern Ontario and New York state. *Sedimentary Geology* 338: 51–71.
Eyles N, McCabe AM, Bowen DQ. 1994. The stratigraphic and sedimentological significance of Late Devensian ice sheet surging in Holderness, Yorkshire, UK. *Quaternary Science Reviews* 13: 727–759.
Eyles N, Putkinen N, Sookhan S, Arbelaez-Moreno L. 2016. Erosional origin of drumlins and megaridges. *Sedimentary Geology* 338: 2–23.
Fannin NGT. 1989. Offshore Investigations 1966-87. British Geological Survey Technical Report WB/89/2.
Feyling-Hanssen RW. 1972. The foraminifer Elphidium excavatum (Terquem) and its variant forms. *Micropaleontology* 18: 337–354.
Gatliff R., Richards P, Smith K, Graham CC, McCormac M, Smith NJP, Long D, Cameron TD, Evans D, Stevenson AG., Bulat J, Ritchie JD. 1994. United Kingdom offshore regional report: the geology of the central North Sea. London: HMSO for the British Geological Survey.
Gilbert R. 1990. Rafting in glacimarine environments. In Glacimarine Environments: Processes and Sediments, Dowdeswell JA, Scourse JD. (eds): Geological Society pf London Spec. Publication 53, 105-120.
Golledge NR, Stoker MS.2006. A palaeo-ice stream of the British Ice Sheet in eastern Scotland. *Boreas* 35: 231–243.
Graham AGC, Lonergan L, Stoker MS. 2007. Evidence for Late Pleistocene ice stream activity in the Witch Ground Basin, central North Sea, from 3D seismic reflection data. *Quaternary Science Reviews* 26: 627–643.
Graham AGC, Stoker MS., Lonergan L, Bradwell T, Stewart MA. 2011. The Pleistocene Glaciations of the North Sea Basin. In Developments in Quaternary Science: Quaternary Glaciations - Extent and Chronology: a Closer Look, Ehlers J, Gibbard PL, Hughes PD (eds): Elsevier, 261–268.
Gravenor CP, Von Brunn V, Dreimanis A. 1984. Nature and classification of waterlain glaciogenic sediments, exemplified by Pleistocene, Late Paleozoic and Late Precambrian deposits. *Earth-Science Reviews* 20: 105–166.
Hansen A, Knudsen KL. 1995. Recent foraminiferal distribution in Freemansundet and Early Holocene stratigraphy on Edgeøya, Svalbard. *Polar Research* 14: 215–238.
Hart JK, Roberts DH. 1994. Criteria to distinguish between subglacial glaciotectonicand glaciomarine sedimentation, I. Deformation styles and sedimentology. *Sedimentary Geology* 91: 1-382
Hedges REM, Housle RA, Law IA, Bronk CR. 1989. Radiocarbon dates from the Oxford AMS system: archaeometry datelist 9. *Archaeometry* 31: 207-234.
Hogan KA, Ó Cofaigh C, Jennings AE, Dowdeswell JA, Hiemstra JF. (2016) Deglaciation of a major palaeo-ice stream in Disko Trough, West Greenland. *Quaternary Science Reviews* 147: 5-26.
Hubbard AL, Bradwell T, Golledge N, Hall A, Patton H, Sugden D, Cooper R, Stoker MS. 2009. Dynamic cycles, ice streams and their impact on the extent, chronology and deglaciation of the British–Irish ice sheet. *Quaternary Science Reviews* 28: 758–776.
Hughes ALC, Clark CD, Jordan CJ. 2014. Flow-pattern evolution of the last British Ice Sheet. *Quaternary Science Reviews* 89: 148–168.
Hughes ALC, Greenwood SL, Clark CD. 2011. Dating constraints on the last British-Irish Ice Sheet: a map and database*. Journal of Maps* 7: 156–184.
Hutton, K. 2018. The glacial geomorphology of the Firth of Forth. Unpublished MRes Thesis. University of Durham.
Huuse M, Lykke-Anderson H. 2000. Over-deepened Quaternary valleys in the eastern Danish North Sea: morphology and origin. *Quaternary Science Reviews* 19: 1233 – 1253.
Iverson NR, Jansson P, Hooke RL. 1994 In situ measurements of the strength of deforming subglacial till. *Journal of Glaciology* 40: 497–503.
Iverson NR. 2010. Shear resistance and continuity of till at glacier beds: hydrology rules. *Journal of Glaciology* 56: 1104-1114.

Jansson KN, Kleman J. 1999. The horned crag-and-tails of the Ungava Bay landform swarm, Québec-Labrador, Canada. *Annals of Glaciology* 28: 168–174.
Jennings CE. 2006. Terrestrial ice streams: a view from the lobe. Geomorphology 75, 100-124.
Jennings AE, Walton ME, Ó Cofaigh C, Kilfeather A, Andrews JT, Ortiz JD, De Vernal A, Dowdeswell JA. 2014. Paleoenvironments during Younger Dryas- Early Holocene retreat of the Greenland Ice Sheet from outer Disko Trough, central west Greenland. *Journal of Quaternary Science* 29: 27–40.
Kilfeather AA, Ó Cofaigh C, Lloyd JM, Dowdeswell, JA, Xu S, Moreto, SG. 2011. Ice-stream retreat and ice-shelf history in Marguerite Trough, Antarctic Peninsula: Sedimentological and foraminiferal signatures. *Geological Society of America Bulletin* 123: 997–1015.
Kneller B, Buckee C. 2000 The structure and fluid mechanics of turbidity currents: a review of some recent studies and their geological implications. *Sedimentology* 47: 62-94.
Kovanen DJ, Slaymaker O. 2004. Glacial imprints of the Okanogan Lobe, southern margin of the Cordilleran Ice Sheet. *Journal of Quaternary Science* 19, 547–565.
Krabbendam M, Glasser NF. 2011. Glacial erosion and bedrock properties in NW Scotland: abrasion and plucking, hardness and joint spacing. *Geomorphology,* 130, 374– 383.
Krabbendam M, Eyles N, Putkinen N, Bradwell T, Arbelaez-Moreno L. 2016. Streamlined hard beds formed by palaeo-ice streams: A review. Sedimentary *Geology* 338: 24–50.
Kristensen L, Benn DI, Hormes A, Ottesen D. 2009. Mud aprons in front of Svalbard surge moraines: Evidence of subglacial deforming layers or proglacial glaciotectonics? *Geomorphology* 111: 206-221.
Lamplugh GW. 1879. On the divisions of the glacial beds in Filey Bay. *Proceedings of the Yorkshire Geological and Polytechnic Society* 1: 161-177.
Livingstone SJ, Ó Cofaigh C, Evans, DJA. 2010. A major ice drainage pathway of the last British-Irish Ice Sheet: the Tyne Gap, northern England. *Journal of Quaternary Science* 25: 354–370.
Livingstone SJ, Evans DJA, Ó Cofaigh C, Davies BJ, Merritt JW, Huddart D, Mitchell WA, Roberts DH, Yorke L. 2012. Glaciodynamics of the central sector of the last British–Irish Ice Sheet in Northern England. *Earth Science Reviews* 111: 25–55.
Livingstone SJ, Roberts DH, Davies BJ, Evans, DJA, Ó Cofaigh C, Gheorghiu DM. 2015. Late Devensian deglaciation of the Tyne Gap Palaeo-Ice Stream, northern England. *Journal of Quaternary Science* 30: 790–804.
Lloyd JM, Park LA, Kuijpers A, Moros M. 2005 Early Holocene palaeoceanography and deglacial chronology of Disko Bugt, West Greenland*. Quaternary Science Reviews* 24: 1741-1755
McCabe AM, Haynes JR, Macmillan NF. 1986. Late-Pleistocene tidewater glaciers and glaciomarine sequences from north County Mayo, Republic of Ireland. *Journal of Quaternary Science* 1: 73–84.
McCabe AM, Knight J, McCarron S. 1998. Evidence for Heinrich Event 1 in the British Isles. *Journal of Quaternary Science* 13: 549–568.
Merritt JW, Connell RE, and Hall AM. 2017. Middle to Late Devensian glaciation of north-east Scotland: implications for the north-eastern quadrant of the last British–Irish ice sheet. *Journal of Quaternary Science* 32: 276–294.
Murray AS, Wintle AG. 2003. The single aliquot regenerative dose protocol: potential for improvements in reliability. *Radiation Measurements 37:* 377-381.
Mulder T, Alexander J. 2001. The physical character of subaqueous sedimentary density flows and their deposits. *Sedimentology* 48: 269-299.
Ó Cofaigh C. 1996. Tunnel valley genesis. *Progress in Physical Geography: Earth and Environment* 20: 1-19.
Ó Cofaigh C, Dowdeswell JA. 2001. Laminated sediments in glacimarine environments: diagnostic criteria for their interpretation. *Quaternary Science Reviews* 20: 1411–1436.
Ó Cofaigh C, Evans DJA. 2001. Sedimentary evidence for deforming bed conditions associated with a grounded Irish Sea glacier, southern Ireland. *Journal of Quaternary Science* 16: 435–454.
Ó Cofaigh C, Dowdeswell JA, Allen CS, Hiemstra JF, Pudsey CJ, Evans J, Evans DJ. 2005. Flow dynamics and till genesis associated with a marine-based Antarctic palaeo-ice stream. *Quaternary Science Reviews* 24: 709–740.

Ottesen D, Dowdeswell JA. 2006. Assemblages of submarine landforms produced by tidewater glaciers in Svalbard. *Journal of Geophysical Research: Earth Surface* 111: F01016, doi:10.1029/ 2005JF000330.
Ottesen D, Dowdeswell JA, Lanvik JY, Mienert J. 2007. Dynamics of the Late Weichselian ice sheet on Svalbard inferred from high-resolution sea-floor morphology. Boreas 36, 286–306.
Patterson CJ. 1997. Southern Laurentide ice lobes were created by ice streams: Des Moines Lobe in Minnesota, USA. *Sedimentary Geology* 111:249-261.
Patterson CJ. 1998. Laurentide glacial landscapes: The role of ice streams. *Geology* 26: 643-646.
Patton, H, Hubbard AL, Andreassen K, Auriac A, Whitehouse PL, Stroeven AP, Shackleton C, Winsborrow MCM, Heyman J, Hall AM. 2017. Deglaciation of the Eurasian ice sheet complex. *Quaternary Science Reviews* 169: 148–172.
Peacock JD, Browne MAE. 1998. Radiocarbon dates from the Errol Beds (pre-Windermere Interstadial raised marine deposits) in eastern Scotland. Quaternary Newsletter 86: 1-7.
Peacock JD. 2002. Macrofauna and palaeoenvironment of marine strata of Windermere Interstadial age on the east coast of Scotland. *Scottish Journal of Geology* 38: 31-40.
Peters JL, Benetti S, Dunlop P, Ó Cofaigh C. 2015. Maximum extent and dynamic behaviour of the last British–Irish Ice Sheet west of Ireland. *Quaternary Science Reviews* 128: 48–68.
Powell RD.1984. Glacimarine processes and inductive lithofacies modelling of ice shelf and tidewater glacier sediments based on Quaternary examples*. Marine Geology* 57(1-4): 1–52.
Powell RD. 1990. Glaciomarine processes at grounding line fans and their growth to ice contact deltas. In Glaciomarine enviroments: processes and sediments, Dowdeswell JA, Scourse JD.(eds): Geological Society Special Publication 52, 53-73.
Powell RD. 2003. Subaquatic landsystems: Fjords: In Glacial landsystems, Evans DJA (ed): Arnold, London, 313 – 347.
Powell RD, Alley RB. 1997. Grounding-Line Systems: Processes, Glaciological Inferences and the Stratigraphic Record. In Geology and seismic stratigraphy of the Antarctic Margin, Barker PF, Cooper AK (eds): *Antarctic Research Series* 2, 169–187.
Powell RD, Domack, EW. 1995. Modern glaciomarine environments. In: Glacial Environments: Volume 1. Modern Glacial Environments: Processes, Dynamics and Sediments, Menzies J. (ed). Butterworth-Heinmann, Oxford, 445–486.
Praeg D. 2003. Seismic imaging of mid-Pleistocene tunnel-valleys in the North Sea Basin – high resolution from low frequencies. *Journal Applied Geophysics* 53: 273–298.
Prescott JR, Hutton JT. 1994. Cosmic ray contributions to dose rates for luminescence and ESR: large depths and long-term time variations. *Radiation Measurements 23*: 497-500.
Roberts DH, Evans DJA., Callard SL, Dove D, Bateman MD, Medialdea A, Saher M, ÓCofaigh C, Chiverrell RC, Moreton SG, Cotterill CJ, Clark, CD. (2018) The MIS II Limit of the British-Irish Ice Sheet in the Southern North Sea. *Quaternary Science Reviews* 198, 181-207
Roberts, DH, Evans, DJA, Lodwick J, Cox NJ. 2013. The subglacial and icemarginal signature of the North Sea Lobe of the British Irish Ice Sheet during the Last Glacial Maximum at Upgang, North Yorkshire, UK. *Proceedings of the Geologists' Association* 124: 503–519.
Scoof C. 2007. Ice sheet grounding line dynamics: Steady states, stability, and hysteresis. Journal of Geophysical research, 112, F03S28, doi:10.1029/2006JF000664.
Sejrup HP, Clark CD, Hjelstuen BO. 2016. Rapid ice sheet retreat triggered by ice stream de-buttressing: Evidence from the North Sea. *Geology* 44: 355–358.
Sejrup HP, Hjelstuen BO, Nygard A, Haflidason H, Mardal I. 2015. Late Devensian ice-marginal features in the central North Sea–processes and chronology. *Boreas* 44: 1-13.
Shreve RL. 1972. Movement of Water in Glaciers. *Journal of Glaciology* 11: 205-214
Slota PJ, Jull AJ, Linick TW, Toolin LJ 1987. *Radiocarbon*, 29, 303-306.
Smith ND, Ashley GM. 1985. Proglacial lacustrine environment, physical processes. In Glacial Sedimentary Environments, Ashley GM, Shaw J, Smith ND (eds): Society of Economic Paleontologists and Mineralogists, Short Course No. 16, 135-217.
Spagnolo M, Clark CD, Ely JC, Stokes, CR, Anderson JB, Andreassen K, Graham AGC, Kin, EC. 2014. Size, shape and spatial arrangement of mega-scale glacial lineations from a large and diverse dataset. *Earth Surface Processes and Landforms* 39: 1432-1448.
Stoker MS, Bent A. 1985. Middle Pleistocene glacial and glaciomarine sedimentation in the west central North Sea. *Boreas* 14: 325 – 332.
Stokes CR, Clark CD. 2001. Palaeo-ice streams. *Quaternary Science Reviews* 20: 1437-1457

Stokes, CR, Clark CD. 2002. Are long subglacial bedforms indicative of fast ice flow? *Boreas* 31: 239-249.
Stokes CR, Fowler AC, Clark CD, Hindmarsh, RCA, Spagnolo M. 2013. The instability theory of drumlin formation and its explanation of their varied composition and internal structure. *Quaternary Science Reviews* 62: 77-96
Talling PJ. 2014. On the triggers, resulting flow types and frequencies of subaqueous sediment density flows in different settings. *Marine Geology* 352: 155-182.
Teasdale D. 2013. Evidence for the western limits of the North Sea Lobe of the BIIS in North East England. In The Quaternary of Northumberland, Durham and Yorkshire Field Guide, Davies BJ, Yorke L, Bridgland DR, Roberts DH (eds): Quaternary Research Association: London, 106–121.
Thomas GSP, Chiverrell RC, Huddart D. 2004. Ice-marginal depositional responses to probable Heinrich events in the Devensian deglaciation of the Isle of Man. *Quaternary Science Reviews* 23: 85–106.
Thomas GSP, Connell RJ. 1985. Iceberg drop, dump, and grounding structures from Pleistocene glacio-lacustrine sediments, Scotland. *Journal of Sedimentary Research* 55: 243-249
Thomsen KJ, Murray AS, Bøtter-Jensen, Kinahan J. 2007. Determination of burial dose in incompletely bleached fluvial samples using single grains of quartz. *Radiation Measurements* 42: 370-379.
Tulaczyk SM, Scherer RP, Clark CD. 2001. A ploughing model for the origin of weak tills beneath ice streams: a qualitative treatment. *Quaternary International* 86: 59–70.
Wood SV, Rome JL. 1868. On the Glacial and Postglacial Structure of Lincolnshire and south-East Yorkshire. *Quarterly Journal of the Geological Society* 24: 2-3.

Tables

Table 1: Radiocarbon ages from offshore cores 118VC, 128VC, 132VC and 137VC. Conventional radiocarbon ages and calibrated ages are shown without marine reservoir correction due to uncertainties over the temporal variation of the marine reservoir effect.

Lab code	**Sample core and depth**	**Geological context and material dated**	**$\delta^{13}C_{VPDB}$‰ (± 0.1)**	**Conventional Radiocarbon Age (years BP ± 2 σ)**	**Calibrated age +/- 2σ** (Cal BP)
SUERC-68009	T2-128VC-280	Laminated glaciomarine seds; Mixed foraminifera assemblage	-1.146	14445 ± 112	16949 ± 216
SUERC-68010	T2-132VC-144	Laminated glaciomarine seds; Mixed foraminifera assemblage	-1.459	16708 ± 130	19571 ± 172
UCIAMS-176372	T2-137VC-552	Laminated glaciomarine seds; Mixed foraminifera assemblage	-1.237	16900 ± 120	19895 ± 218
SUERC-68001	T2- 118VC- 240a	Laminated glaciomarine seds; Nuculana pernula	0.470	15157 ± 120	17862 ± 169
SUERC-68007	T2_118VC_240b	Laminated glaciomarine seds; Mixed foraminifera assemblage	-1.845	14206 ± 114	16529 ± 235

Table 2. OSL age data for samples from glacial outwash sediments at Seaham, County Durham. These sit between the Blackhall and Horden Tills are therefore represent deposition along the western NSL ice margin

just prior to final deglaciation. Data includes palaeomoisutre (w), total dose rate, number of aliquots measured and accepted in brackets, the derived estimated equivalent doses (D_e) and resultant ages.

Lab code	Field code	W (%)	Beta dose rate (Gy/ka)	Gamma dose rate (Gy/ka)	Total dose rate (Gy/ka)	n	D_e (Gy)*	OD (%)	Age (ka)
Shfd14064	Sea14/1/1	23	539 ± 43	586 ± 31	1.14 ± 0.05	91 (47)	22.6 ± 1.8	72	19.8 ± 1.8
Shfd14065	Sea14/1/2	23	539 ± 41	569 ± 31	1.13 ± 0.05	92 (47)	21.7 ± 1.4	93	19.1 ± 1.9
Shfd14066	Sea14/1/3	23	465 ± 36	710 ± 40	1.12 ± 0.05	66 (35)	23.8 ± 2.5	83	19.9 ± 2.3

***** De derived using IEU

Table 3: Calibrated radiocarbon ages from the periphery of the Tay and Forth estuaries. With the exception of the site at Shiells all sites mark the onset of glaciomarine conditions with ice receding westward and onshore (note no adjustment for marine reservoir) (see Hughes et al., 2011 for overview)

Site	Lab code	Geological context and material dated	Calibrated age (no mar res correction)	± error	Source
Shiells	SRR-391	Terrestrial ice free conditions; organics	16,444	205	Peacock & Browne 1998; Harkness & Wilson 1979
Gallowflat	AA-37787	Errol BedsFm; -Glaciomarine; Rabilimis mirabilis and Heterocyprideis sorbyana	16,693	132.5	Peacock 2002
Gallowflat	Beta-111508	Errol Beds Fm; Glaciomarine; Portlandia arctica	16,000	130	Peacock 2002
Gallowflat	CAMS-77912	Errol BedsFm; Glaciomarine; Benthic foraminifera	16,786	137.5	Peacock 2002
Barry Clay Pit	OxA-1704	Errol Beds Fm; Glaciomarine; Balanus sp.	16,898	273.5	Peacock & Browne 1998; Hedges et al. 1989
Kinneil Kerse	OxA-1347	Kinneil Kerse Fm overlying Errol Beds Fm; Marine; Nuculana pernula	15,488	190 -	Hedges et al. 1989; Peacock 1999

Figure Captions

Fig. 1. A bathymetric overview of the North Sea showing the position of BIIS and FIS ice margins, flowlines and ice divides during MIS 2 glaciation. The NSL was distinctive lobe of ice that flowed southeast from the Firth of Forth region towards Norfolk in eastern England towards the end of MIS 2 glaciation. It's seafloor imprint has often been correlated to the distribution of Bolders Bank Formation (BDK) sediment, but controls on its hypsometry, dynamic behaviour and recession are poorly constrained. Major drainage basins feeding the NSL include the Firth of Forth, Tweed (Tw), Tyne Gap (Ty) and the Eden-Stainmore (Ed-St) gap (Image based on reconstruction of Dove et al., 2017 and Roberts et al. 2018).

Fig. 2. a) The bedrock geology of the floor of the central western North Sea. Close to the Durham coast. Carboniferous, Permian and Triassic rocks are prevalent. b) The drift geology of the central western North Sea. Note the distribution of the Wee Bankie and Bolders Bank Formations which delimit the footprint of the North Sea Lobe.

Fig. 3. a) The bathymetry of the central western North Sea close to the north east coast of England. The areas immediately offshore between Seaham and Eyemouth are very shallow but deepen to 113m in the central study area. b) Several distinctive landforms can be mapped across the seafloor. They include sediment wedges and ridges, lineations, channels and bedrock ridges.

Fig. 4. Sub-bottom profile data gathered from the study area. Note the position of several bedrock ridges (R1-24); sediment wedges W1 and W2 and ridges M1. Five distinctive acoustic facies can be mapped (AF 1-5). AF1 is bedrock. AF2 and AF3 are diamictic, while AF4 is a stratified/laminated sediment package composed of fines. AF5 is a sandy facies with a distinctive reworked shell assemblage. a) Acoustic data from the seafloor between core 128 VC and 136VC running NW to SE across the study area. b) Acoustic data from the seafloor between core 132VC and 133VC and the area from 134VC to 135VC (see Fig 3a for location of cores).

Fig. 5. Acoustic facies mapped across the study area. AF1 varies with bedrock type. AF2 and AF3 are acoustically opaque and structureless, though AF2 has a slightly more transparent quality. They are plastered across the underlying bedrock. Core samples show them to be diamictic in nature. AF3 forms the core of several grounding zone wedges. AF4 is a stratified sediment package that infills local basinal topography and drapes the underlying sediments. AF5, where present, is a thin and transparent. It occasional forms small sand ridges.

Fig. 6. Acoustic facies mapped at each core location. Most cores penetrate AF4 but only just reach AF3.

Fig. 7. a) Core JC123-128VC with paired photographs and X-ray images. The base of the core is diamictic (AF3) but grades upwards in to a laminated clay/silt with a decreasing in clast content (AF4). It is capped by a sandy/shelly deposit (AF5). A radiocarbon date from 280cm down core provided an age of 16.9 ka cal. BP. b) Core123-132VC; The lower laminated sediments in this core (AF4) provide at radiocarbon age of 19.5 ka cal. BP. They are truncated by a massive diamict mid core before grading back into AF4.

Fig. 8. a) Core JC123-135VC with paired photographs and X-ray images. This core typifies many in the study area with a lower massive diamict (AF3) grading upwards into a stratified diamict before the sediments become intensely laminated (AF4). The lack of clasts in the laminated sediments suggest a lack of ice rated input during deglaciation. The core is capped by a distinctive sandy/shelly deposit (AF5). b) Foraminiferal counts form core JC123-135VC. *Elphidium excavatum (clavatum*) and *Cassidulina reniforme* are known indicators of extreme glacial marine environments, and other indicator species such as *Elphidium incertum, Elphidium asklundi*, *Elphidium albiumbilicatum, Haynesina orbiculare* and *Bolivina sp*. further corroborate cold glaciomarine conditions.

Fig 9. a) Core JC123-136VC – the lowest section of this core exhibits clear evidence for current reworking on the seafloor cross lamination, micro-ripples, and micro cut and fill structures suggesting underflow activity. b) Core JC123-137VC (see Fig. 17 for locality) has a 5m sequence of glaciomarine sediments similar in character to AF4. A radiocarbon date from the base of the core provides an early deglacial age of 19.9 ka cal. BP.

Fig. 10. The glacial stratigraphy form a coastal section at Seaham, County Durham. The section has two glacial diamicts separated by a glacial fluvial sand. These sediments cannot be directly related to the offshore acoustic stratigraphy as the near shore areas have been scoured of glacial sediment, but glaciofluvial sands provide three OSL ages that limit final deglaciation of the coast by the NSL to after 19.6 ka.

Fig. 11. a) A bathymetry cross profile across a series of mega-scale glacial lineations. Drift/bedrock cores not differentiated. b) Partially buried bedrock ridges. Where drift is slightly thicker their surface form is more subdued. c) In some localities glaciogenic sediment constitutes the whole bedform forming drumlins (pink = bedrock; purple = diamict AF3; fuschia =

drift drumlin core. d) BGS seismic line 1993-1/1close to the Northumberland coast. Note the buried streamlined bedforms. The have drumlin-like dimensions but have been previously interpreted as buried dunes by Brew (1996).

Fig 12. Streamlined bedforms in drift across the seafloor north of core 132VC. Some, but not all, bedforms appear to be seeded from perturbations on the seabed. It is also possible to see that some ridges are more ovate in planform. Yellow areas are bedrock highs with very thin glacial sediment cover. See Figure 3 for locational information.

Fig. 13. a-c) Distinctive channels cut into bedrock in the northern part of the study area running NW to SE (parallel to former ice flow direction). C3 – C5 are anastomosing and interconnected. C2 is up to 10 m deep and has an up/down long profile.

Fig. 14. The bedrock geology offshore from Durham/Northumberland showing the structural geology of the region compared to the distribution of glacial landforms. Transverse bedrock ridges trending NE to SW are prominent across the seafloor and formed in Carboniferous, Permian and Triassic rocks. They are controlled by orientation of synclines, faults or regional igneous intrusions. MSGL occur mainly occur Permian and Triassic bedrock but the juxtaposition of both bedrock-cored and sediment-cored bedforms reinforces the notion that in areas of thin sediment cover the subglacial bed is partially emergent and partially inherited with bedforms evolving via a combination of erosion, deposition and deformation.

Fig 15. The mixed-bed glacial landsystem of the NSL during deglaciation under marine conditions. An irregular, scoured and eroded bedrock surface forms the base of the sequence. Subglacial sediments form discontinuous till sheets which feed grounding zone wedges. These are later draped by proximal and distal glaciomarine sediments as the margin actively retreats. The presence of an ice shelf is, as yet, unsubstantiated.

Fig 16. The NSL imprint in this region has characteristics of both hard and soft bed processes; it is a mixed-bed subglacial landsystem. It is a product of an ice stream lobe undergoing rapid transition from a terrestrial piedmont-lobe margin with a net surplus of sediment to the south, to a dynamic, quasi-stable, tidewater margin as the ice withdrew northwards. Grounding line instabilities, drawdown and enhanced flow velocities triggered by marine inundation of the North Sea would have been the most influential feedbacks controlling the development of the mixed-bed signal during deglaciation; bed excavation to partial bedrock, increasing bed roughness, till advection and GZW construction all being the knock-on effects of grounding line instability.

Fig 17. The retreat of the NSL based on new and existing radiocarbon and OSL ages from the east coast of the UK and the offshore areas of Durham and Northumberland. The NSL departed the north Norfolk coast after 22.8 – 21.5 ka BP, leaving till wedges and arcuate moraine complexes on the seafloor as it migrated northwards (green lines; Dove et al. 2017; Roberts et al., 2018). New dates from the Durham area and offshore suggest the ice margin became quasi-stable as a large grounding zone wedge developed (W1) at sometime around 19.5 – 19.9 ka. W2 and moraine complex M1 also suggest further periods of ice marginal stability before the NSL retreated into the Firth of Forth between 17.8 and 16.0 ka cal. BP.

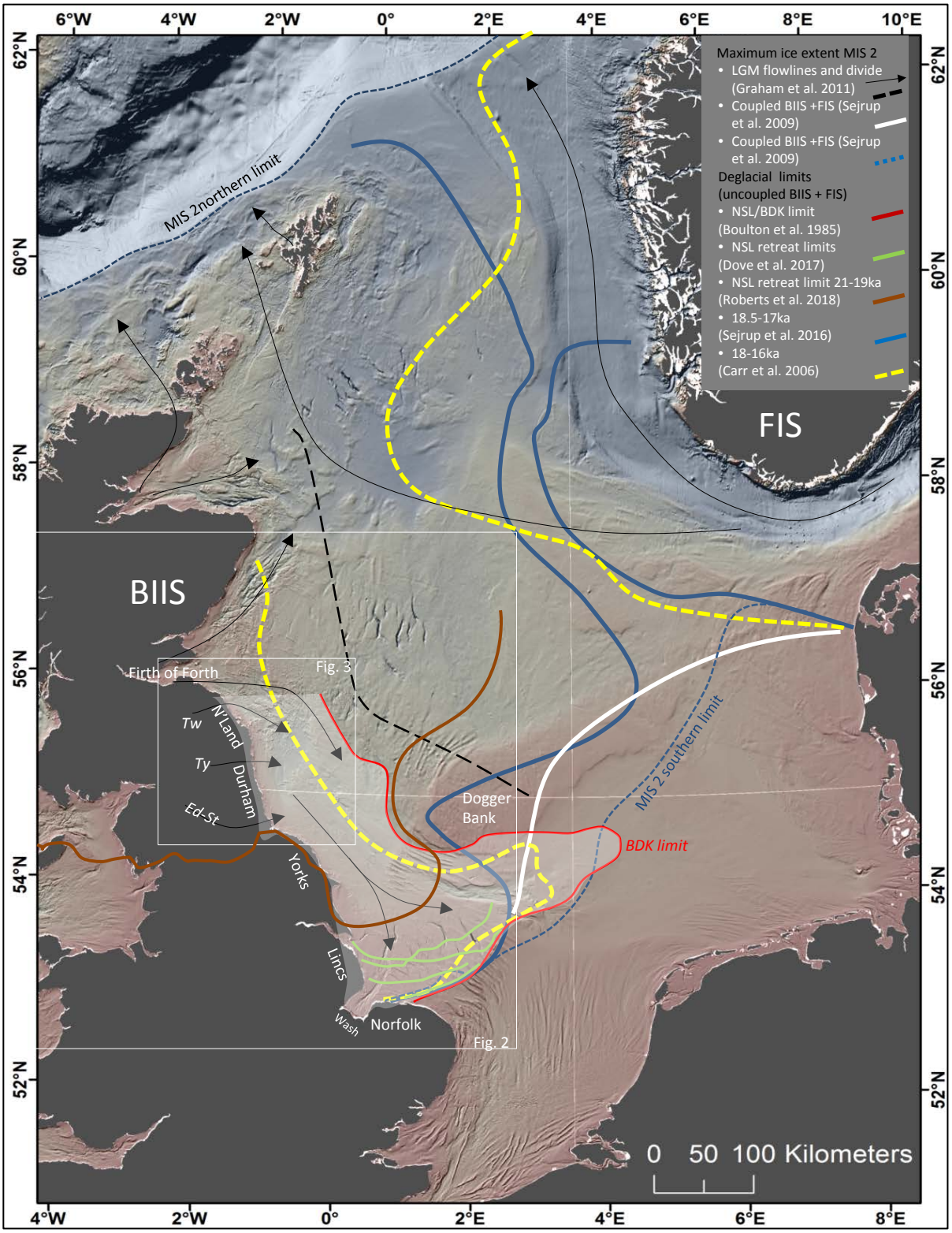
Maximum ice extent MIS 2
• LGM flowlines and divide (Graham et al. 2011)
• Coupled BIIS +FIS (Sejrup et al. 2009)
• Coupled BIIS +FIS (Sejrup et al. 2009)
Deglacial limits (uncoupled BIIS + FIS)
• NSL/BDK limit (Boulton et al. 1985)
• NSL retreat limits (Dove et al. 2017)
• NSL retreat limit 21-19ka (Roberts et al. 2018)
• 18.5-17ka (Sejrup et al. 2016)
• 18-16ka (Carr et al. 2006)
MIS 2northern limit
FIS
BIIS
Firth of Forth
Fig. 3
Tw
N'Land
Ty
Durham
Ed-St
Dogger Bank
MIS 2 southern limit
BDK limit
Yorks
Lincs
Wash
Norfolk
Fig. 2
0 50 100 Kilometers
6°W
4°W
2°W
0°
2°E
4°E
6°E
8°E
10°E
62°N
60°N
58°N
56°N
54°N
52°N

Fig. 1

a)

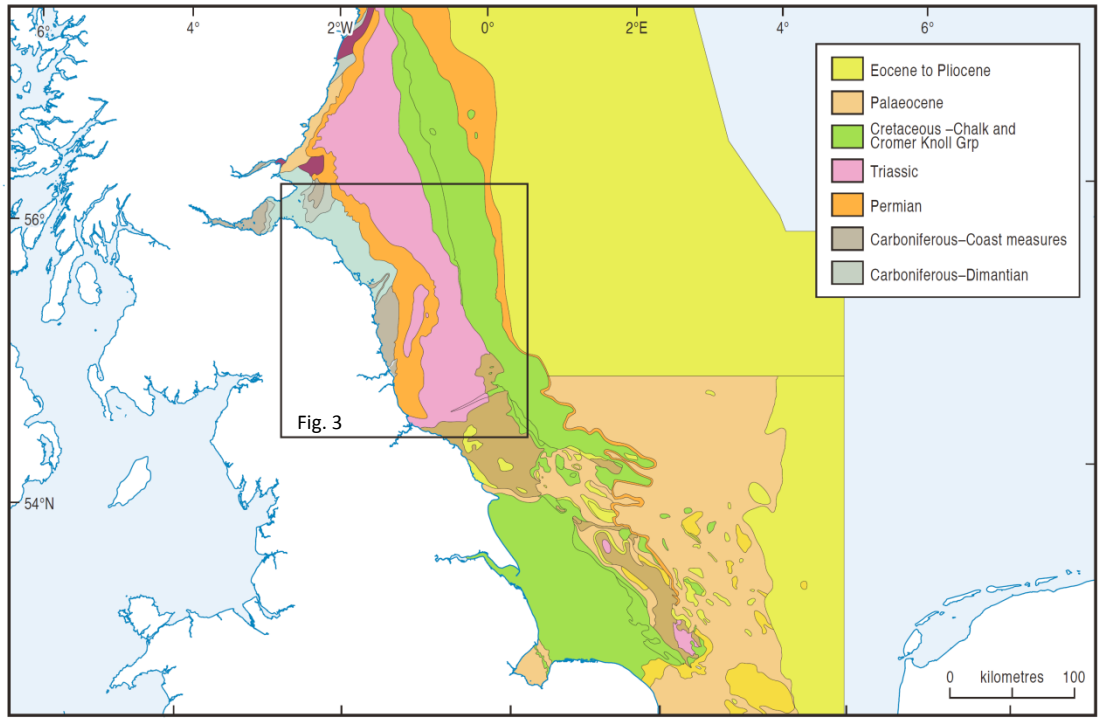
6°
4°
2°W
0°
2°E
4°
6°
56°
54°N
Fig. 3
Eocene to Pliocene
Palaeocene
Cretaceous –Chalk and Cromer Knoll Grp
Triassic
Permian
Carboniferous–Coast measures
Carboniferous–Dimantian
0 kilometres 100

b)

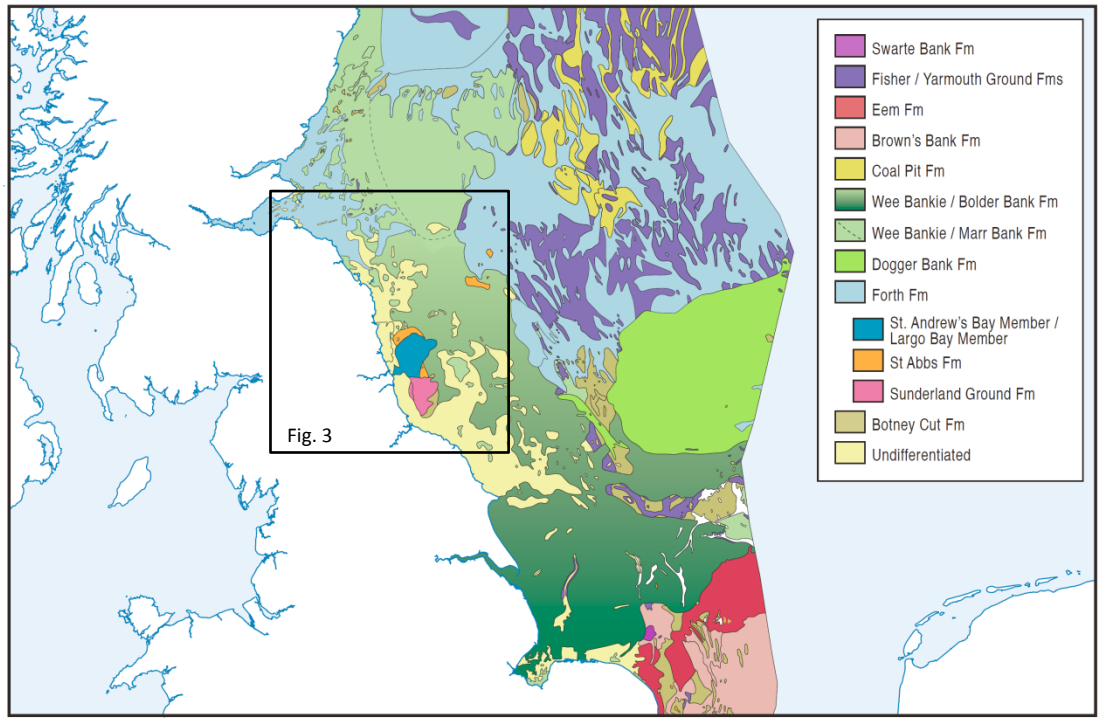
Fig. 3
Swarte Bank Fm
Fisher / Yarmouth Ground Fms
Eem Fm
Brown's Bank Fm
Coal Pit Fm
Wee Bankie / Bolder Bank Fm
Wee Bankie / Marr Bank Fm
Dogger Bank Fm
Forth Fm
St. Andrew's Bay Member / Largo Bay Member
St Abbs Fm
Sunderland Ground Fm
Botney Cut Fm
Undifferentiated

Fig. 2

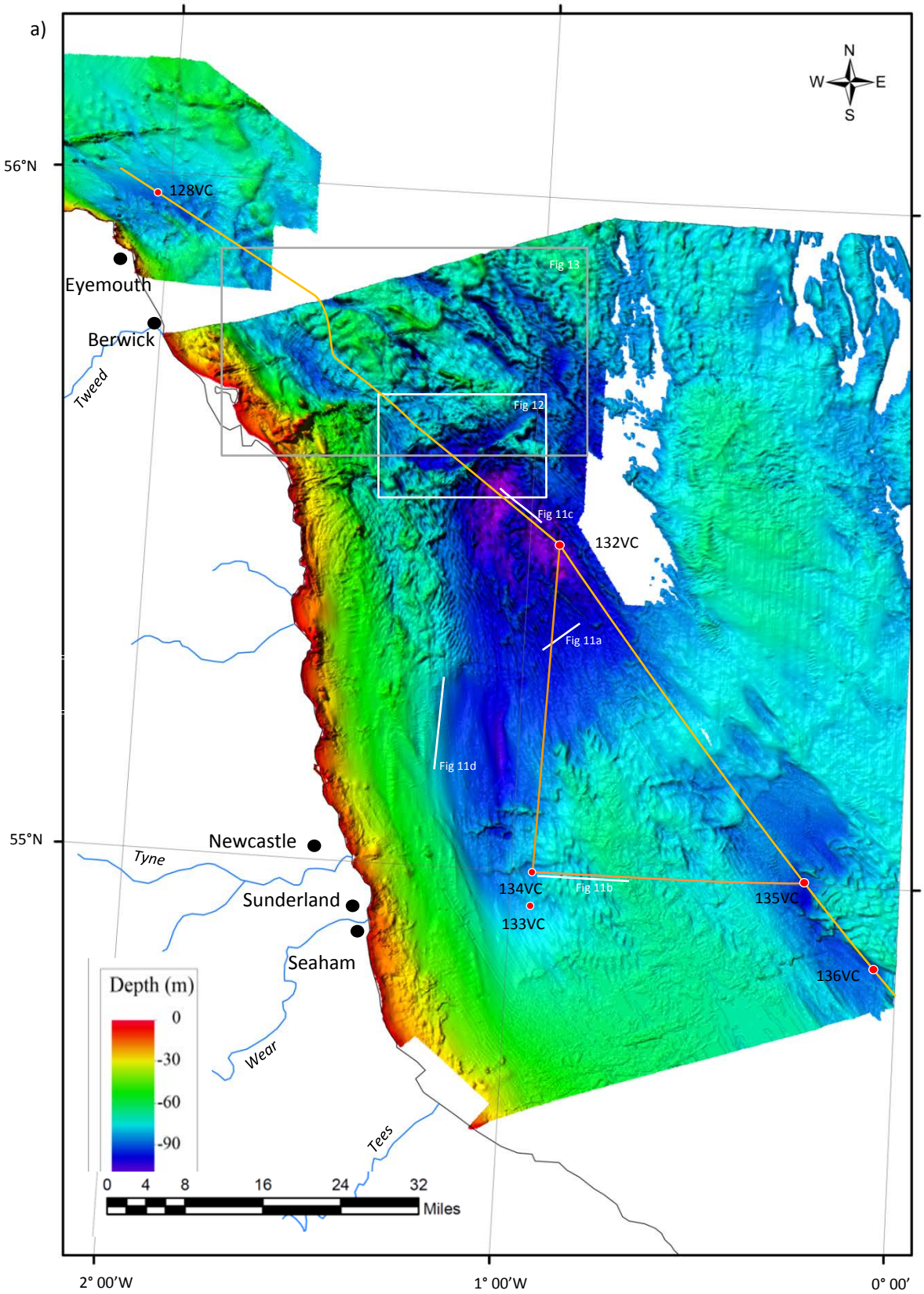
a)
N
W
E
S
56°N
55°N
128VC
Eyemouth
Berwick
Tweed
Fig 13
Fig 12
Fig 11c
132VC
Fig 11a
Fig 11d
Newcastle
Tyne
Sunderland
Seaham
Wear
Tees
134VC
Fig 11b
133VC
135VC
136VC
Depth (m)
0
-30
-60
-90
0 4 8 16 24 32
Miles
2° 00'W
1° 00'W
0° 00'

Fig. 3a

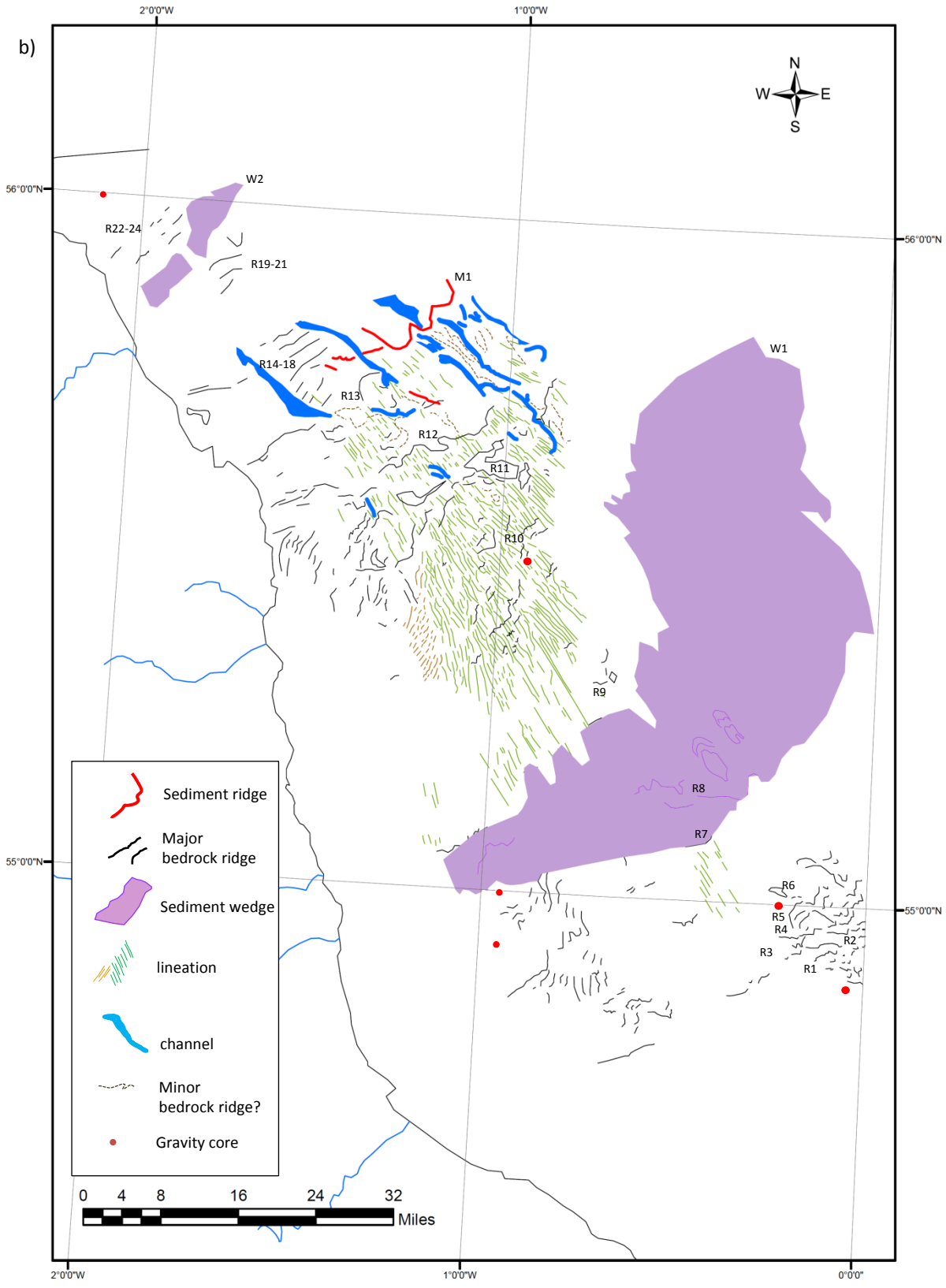
b)
2°0'0"W
1°0'0"W
0°0'0"
56°0'0"N
55°0'0"N
N
W
E
S
W2
R22-24
R19-21
M1
R14-18
R13
R12
R11
R10
W1
R9
R8
R7
R6
R5
R4
R3
R2
R1
Sediment ridge
Major bedrock ridge
Sediment wedge
lineation
channel
Minor bedrock ridge?
Gravity core
0 4 8 16 24 32
Miles

Fig. 3b

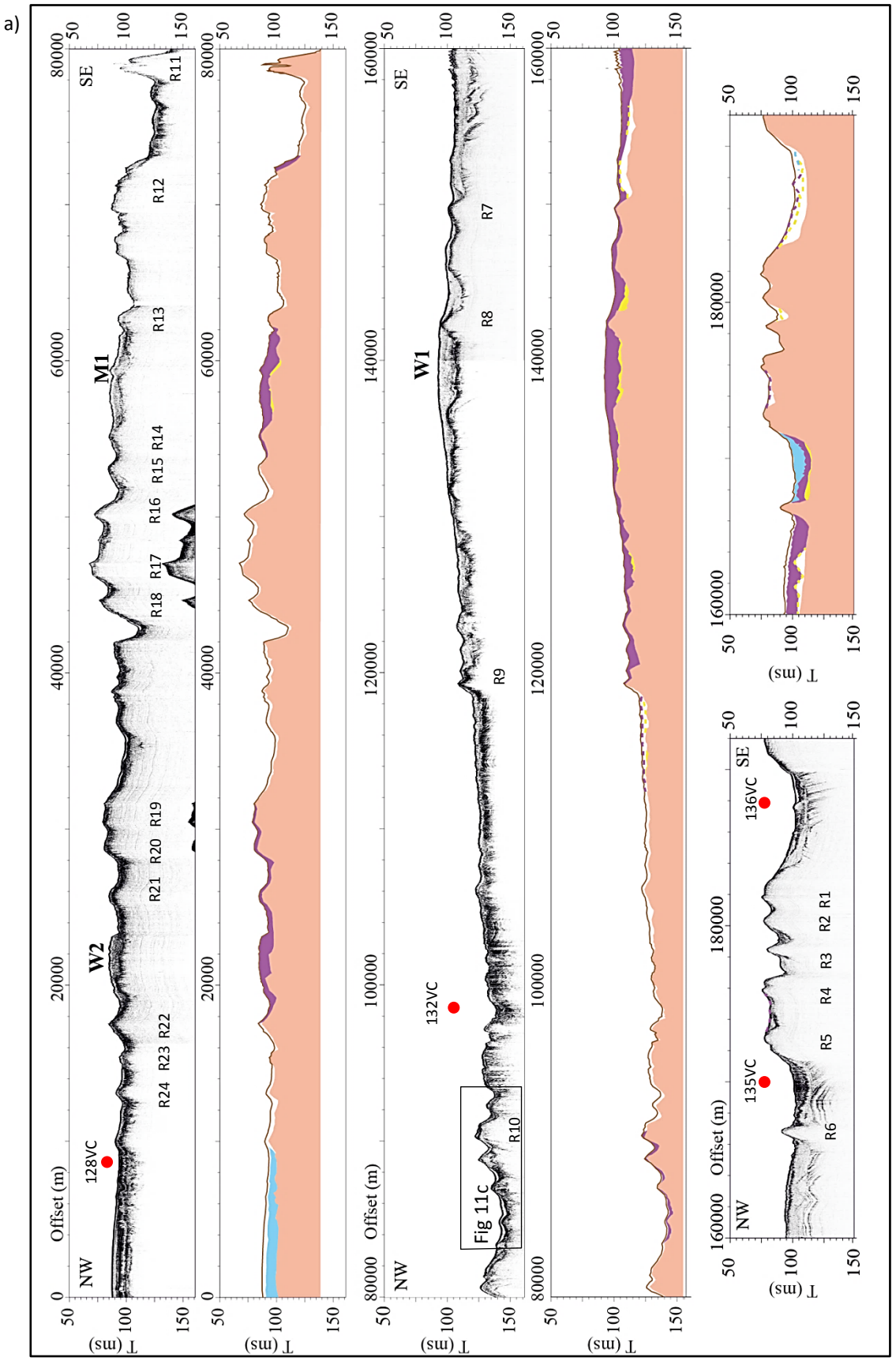
a)
NW
SE
Offset (m)
T (ms)
128VC
132VC
135VC
136VC
W1
W2
M1
R1
R2
R3
R4
R5
R6
R7
R8
R9
R10
R11
R12
R13
R14
R15
R16
R17
R18
R19
R20
R21
R22
R23
R24
Fig 11c

Fig. 4a

b)

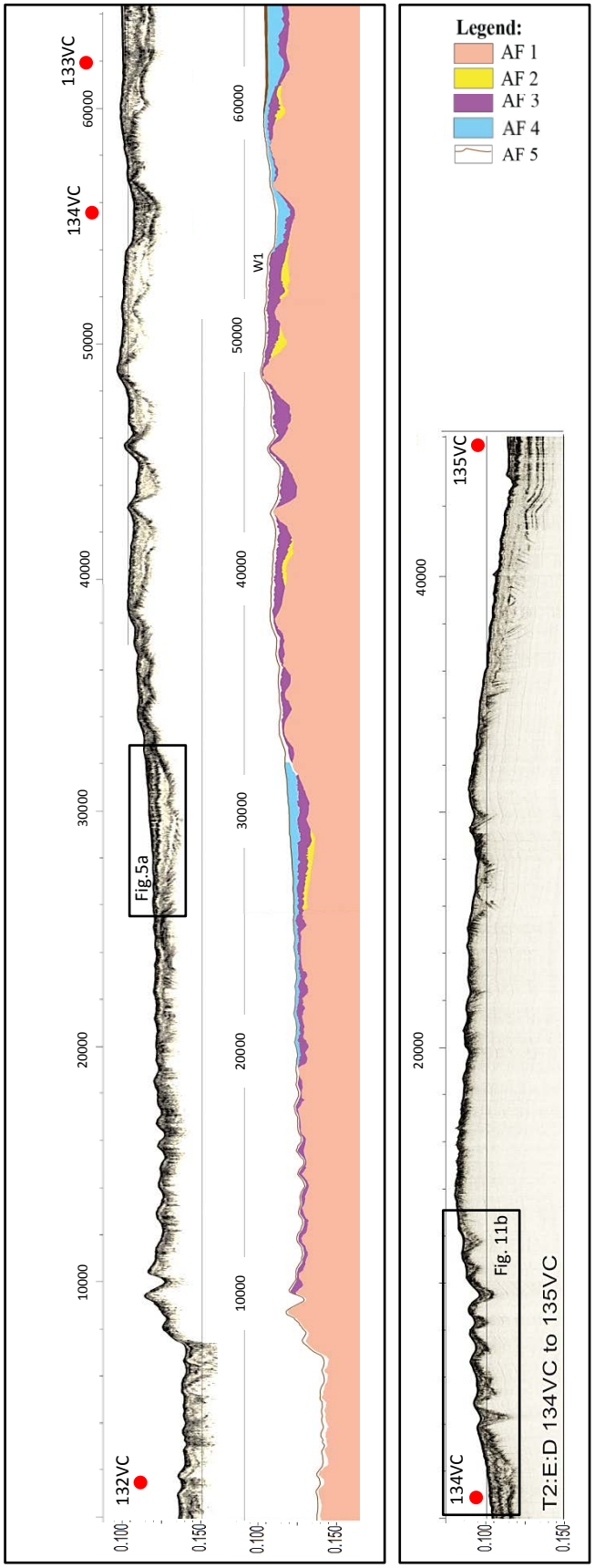
Legend:
AF 1
AF 2
AF 3
AF 4
AF 5
132VC
133VC
134VC
135VC
W1
Fig.5a
Fig. 11b
T2:E:D 134VC to 135VC
10000
20000
30000
40000
50000
60000
0.100
0.150

Fig. 4b

a)

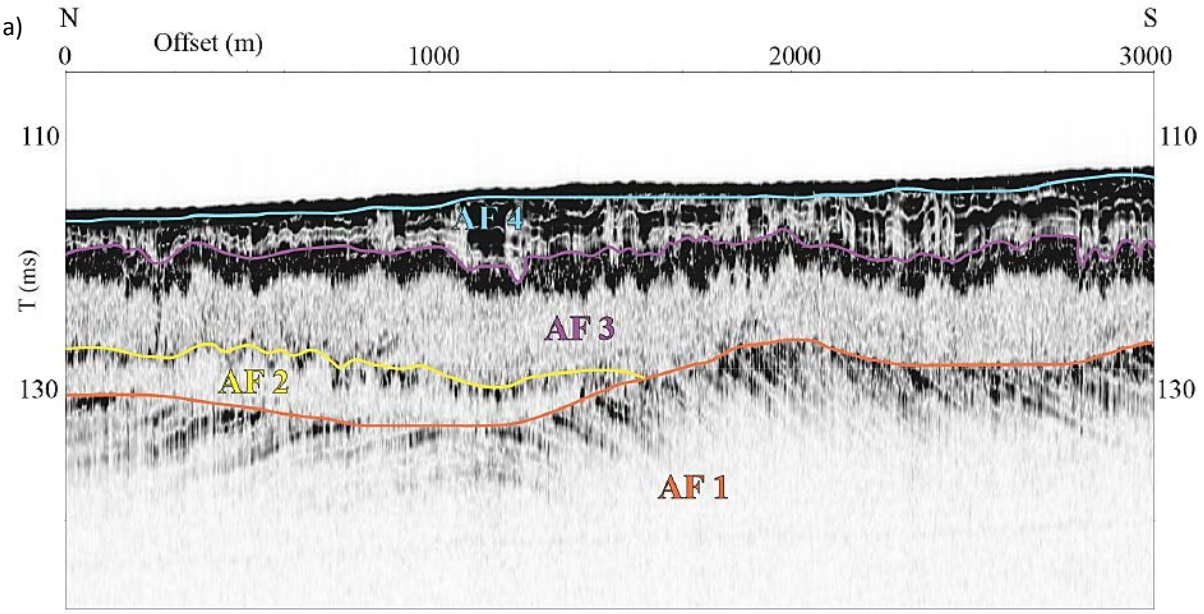

b)

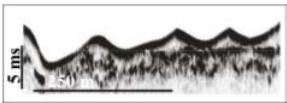	High amplitude seafloor reflector	AF 5
	High frequency and amplitude parallel reflectors that appear deformed	AF 4
	High amplitude and irregular upper boundary. Opaque internal appearance	AF 3
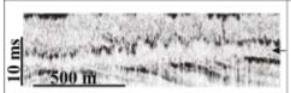	Irregular and discontinuous upper boundary. Transparent internal appearance	AF 2
	High amplitude parallel reflectors which appear faulted and folded	AF 1e (Cretaceous)
	High amplitude parallel reflectors which at times appear folded and faulted	AF 1d (Jurassic)
	High amplitude and frequency parallel reflectors, which appear folded and faulted	AF 1c (Triassic)
	Highly deformed, irregular and discontinuous parallel reflectors	AF 1b (Permian)
	Folded and faulted, low amplitude parallel reflectors	AF 1a (Carboniferous)

Fig. 5

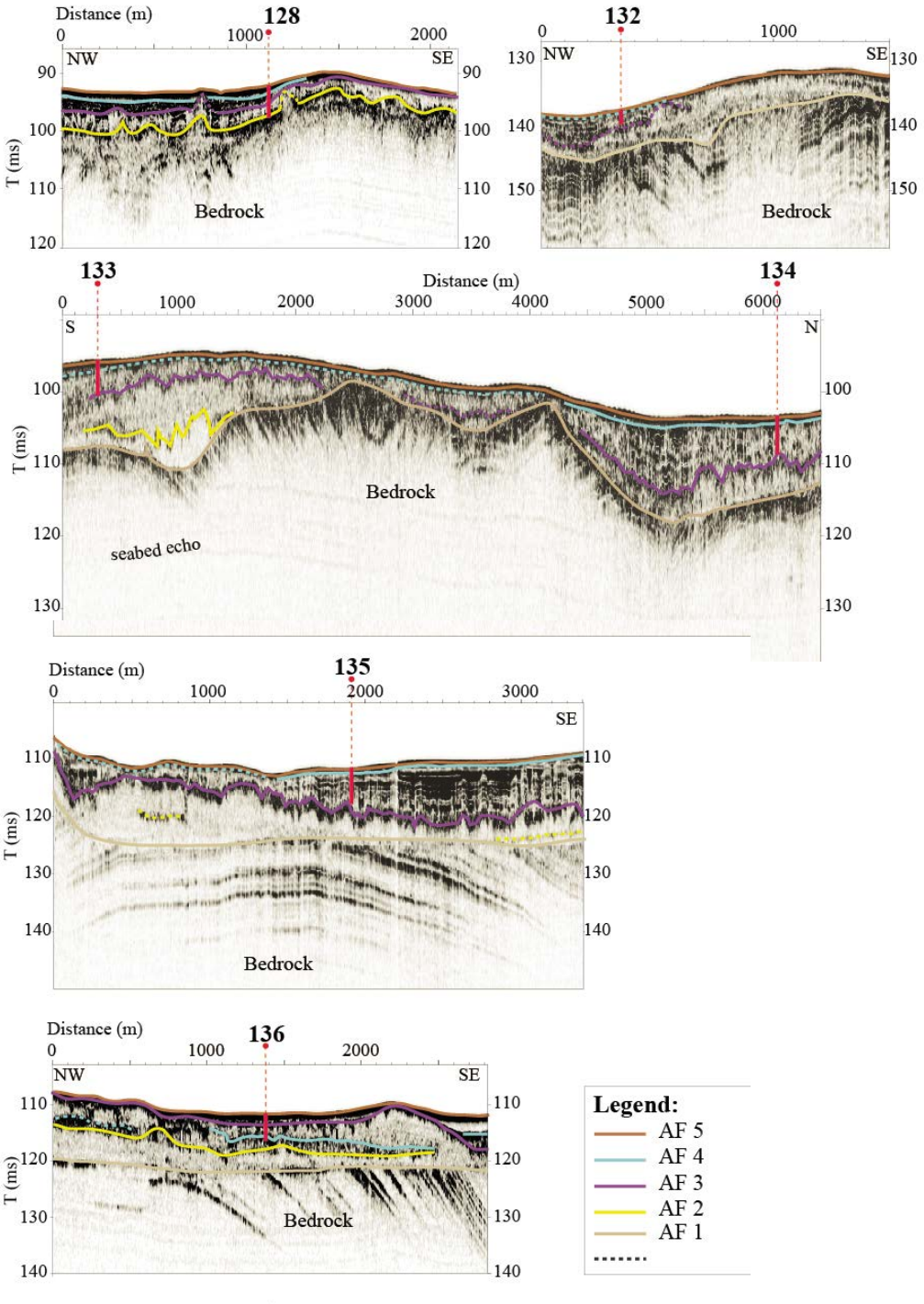
Distance (m)
128
0
1000
2000
NW
SE
90
100
110
120
T (ms)
Bedrock
132
130
140
150
133
134
3000
4000
5000
6000
S
N
seabed echo
135
136
Legend:
AF 5
AF 4
AF 3
AF 2
AF 1

Fig. 6.

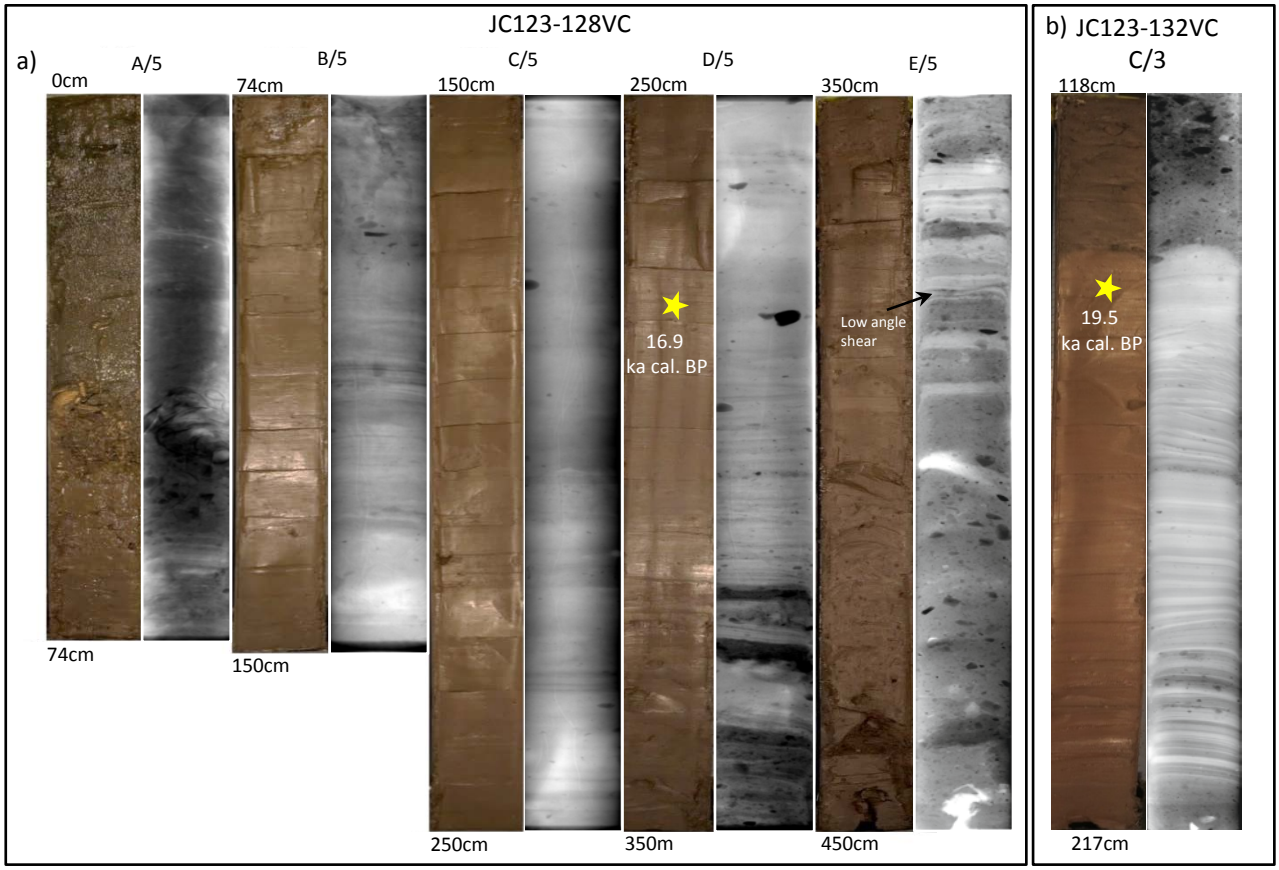
JC123-128VC
a)
A/5
B/5
C/5
D/5
E/5
0cm
74cm
150cm
250cm
350cm
74cm
150cm
250cm
350m
450cm
16.9
ka cal. BP
Low angle
shear
b) JC123-132VC
C/3
118cm
19.5
ka cal. BP
217cm

Fig. 7

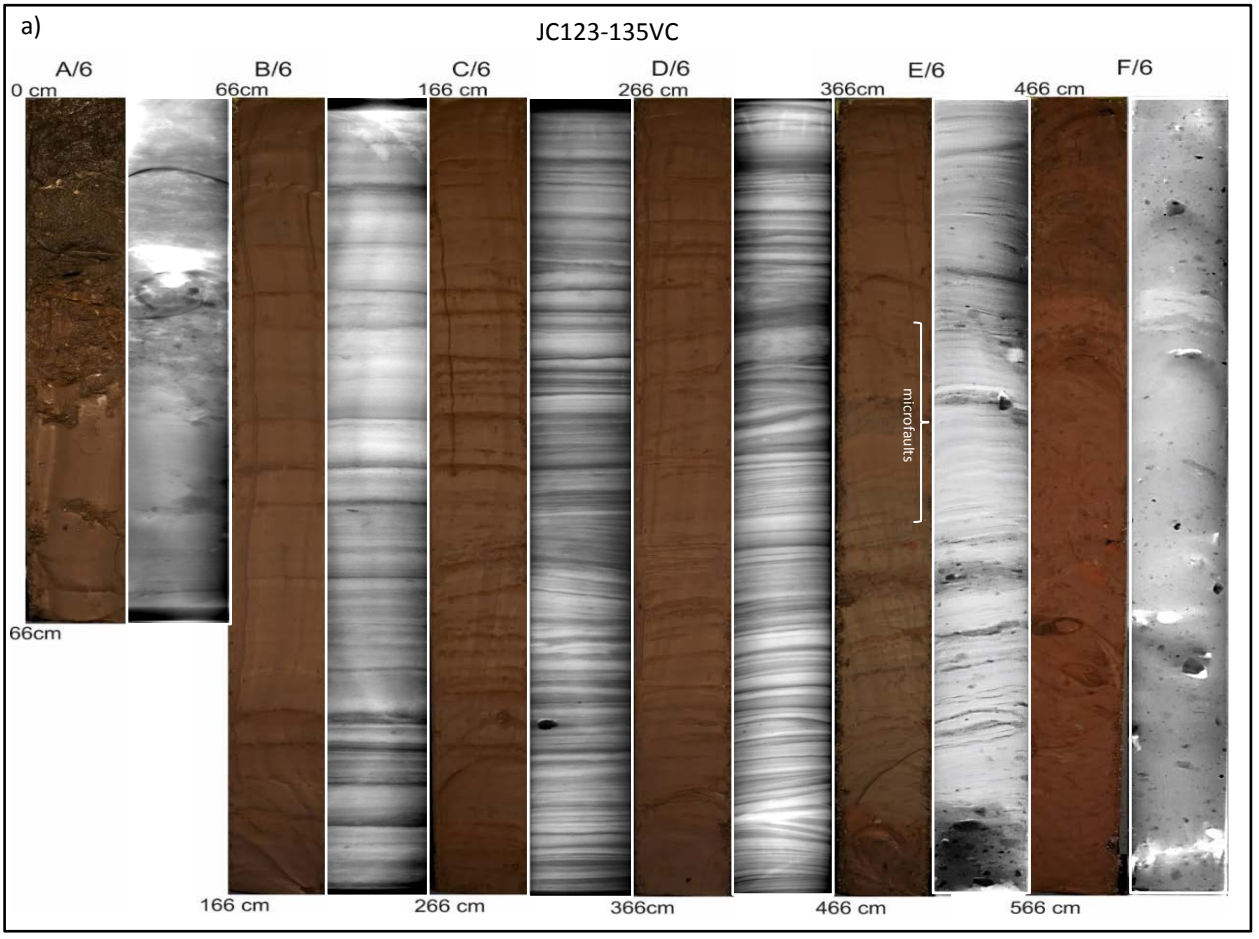
a)
JC123-135VC
A/6
B/6
C/6
D/6
E/6
F/6
0 cm
66cm
166 cm
266 cm
366cm
466 cm
microfaults
66cm
166 cm
266 cm
366cm
466 cm
566 cm

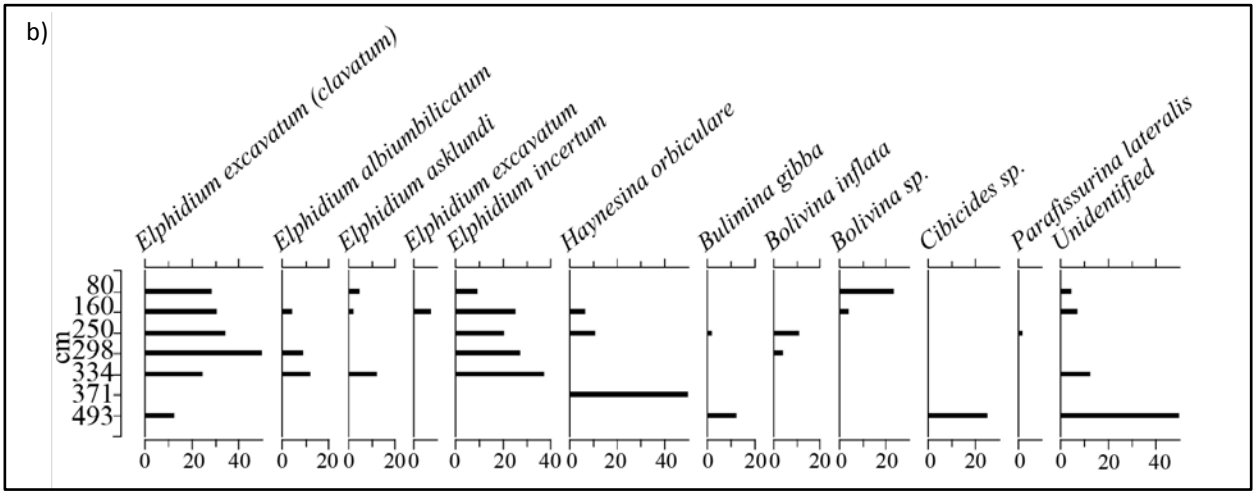
b)
Elphidium excavatum (clavatum)
Elphidium albiumbilicatum
Elphidium asklundi
Elphidium excavatum
Elphidium incertum
Haynesina orbiculare
Bulimina gibba
Bolivina inflata
Bolivina sp.
Cibicides sp.
Parafissurina lateralis
Unidentified
cm
80
160
250
298
334
371
493
0 20 40
0 20
0 20
0 20 40
0 20 40
0 20
0 20
0 20
0 20
0 20
0 20 40

Fig. 8

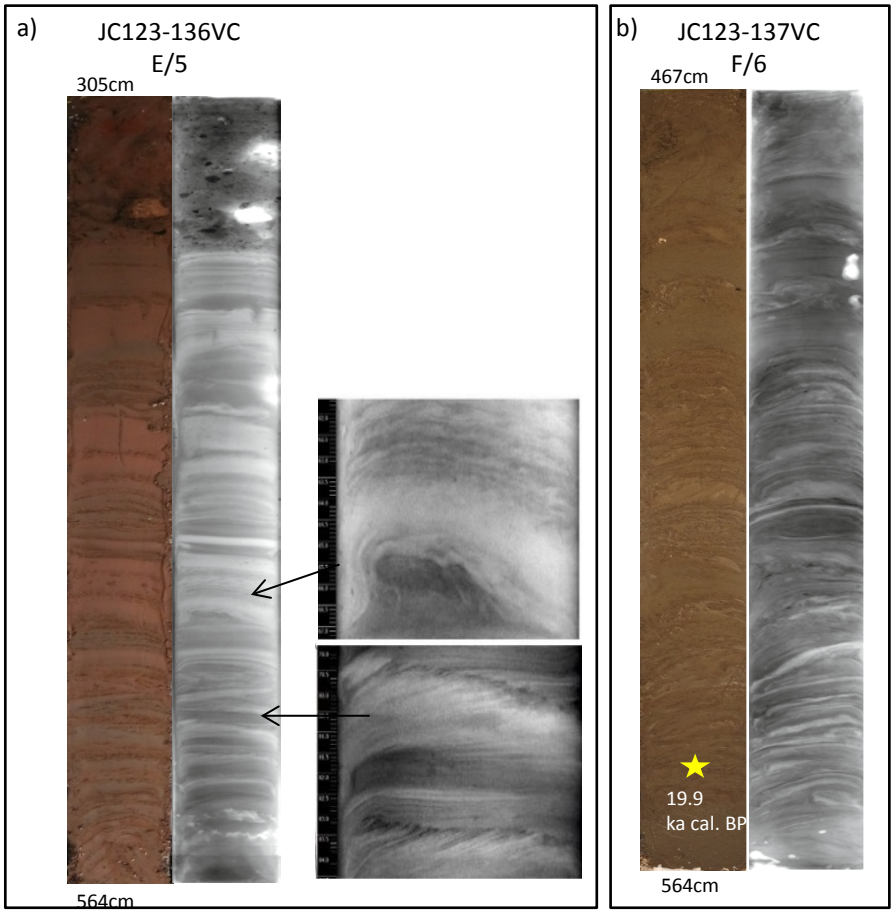
a)
JC123-136VC
E/5
305cm
564cm
b)
JC123-137VC
F/6
467cm
19.9
ka cal. BP
564cm

Fig. 9

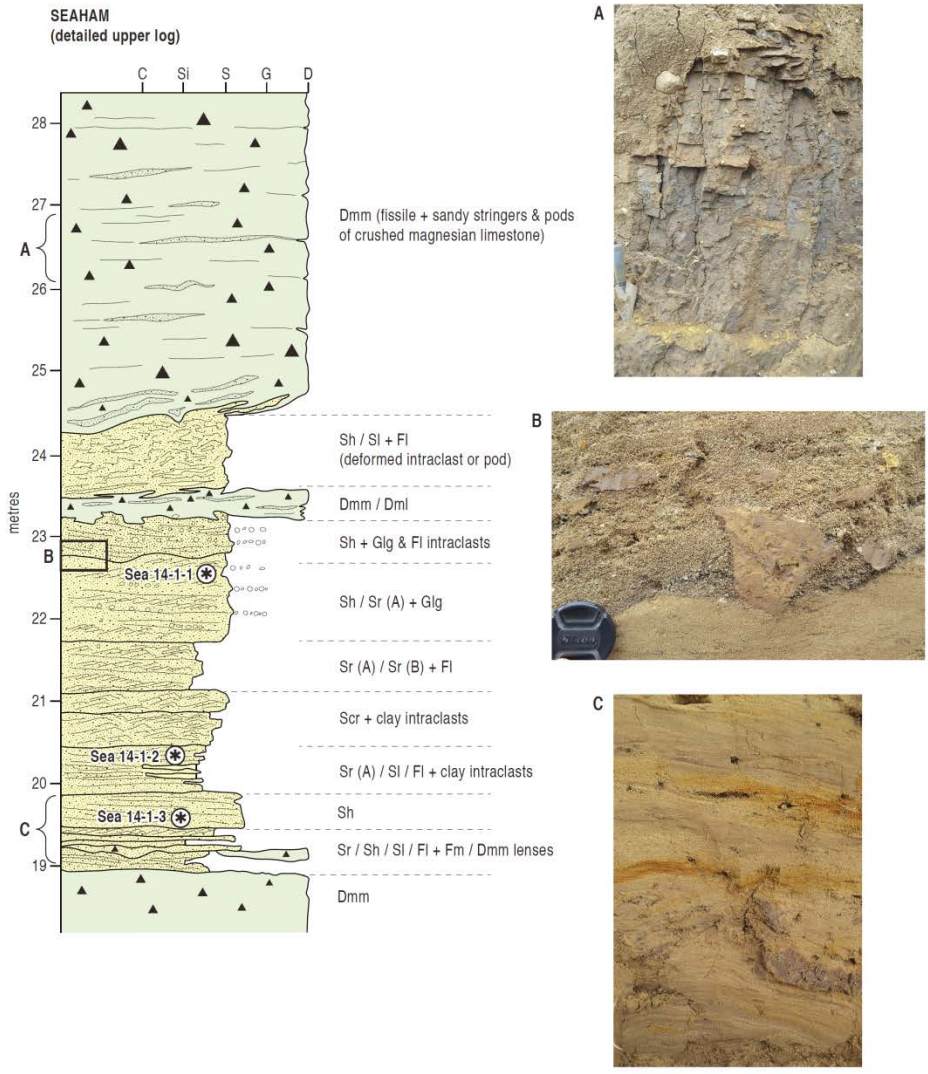
SEAHAM
(detailed upper log)
C
Si
S
G
D
28
27
26
25
24
23
22
21
20
19
metres
A
B
C
Sea 14-1-1
Sea 14-1-2
Sea 14-1-3
Dmm (fissile + sandy stringers & pods of crushed magnesian limestone)
Sh / Sl + Fl (deformed intraclast or pod)
Dmm / Dml
Sh + Glg & Fl intraclasts
Sh / Sr (A) + Glg
Sr (A) / Sr (B) + Fl
Scr + clay intraclasts
Sr (A) / Sl / Fl + clay intraclasts
Sh
Sr / Sh / Sl / Fl + Fm / Dmm lenses
Dmm
A
B
C

Fig. 10

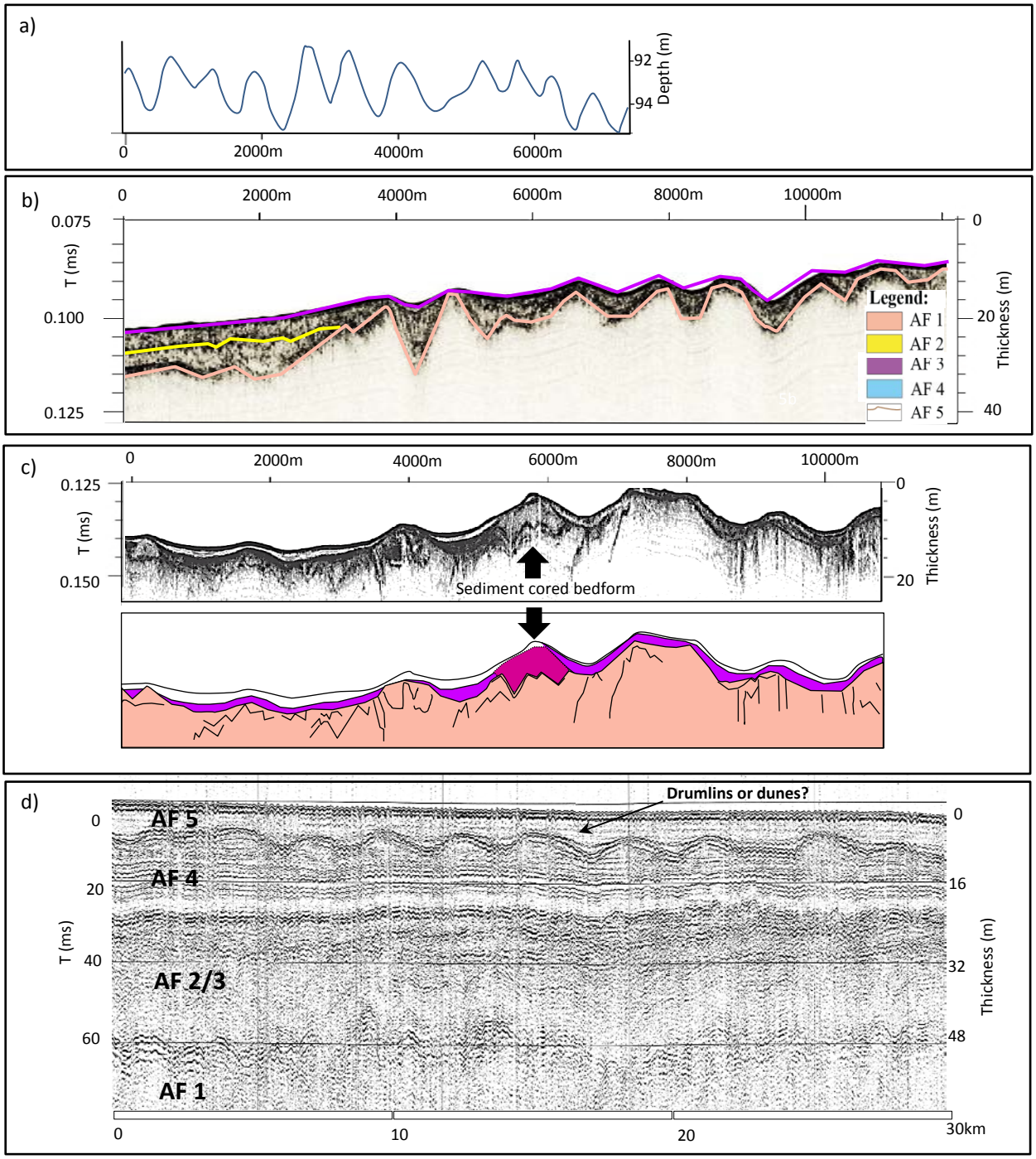
a)
92
94
Depth (m)
0
2000m
4000m
6000m
b)
0
2000m
4000m
6000m
8000m
10000m
0.075
0.100
0.125
T (ms)
0
20
40
Thickness (m)
Legend:
AF 1
AF 2
AF 3
AF 4
AF 5
c)
0
2000m
4000m
6000m
8000m
10000m
0.125
0.150
T (ms)
0
20
Thickness (m)
Sediment cored bedform
d)
Drumlins or dunes?
AF 5
AF 4
AF 2/3
AF 1
0
20
40
60
T (ms)
0
16
32
48
Thickness (m)
0
10
20
30km

Fig. 11

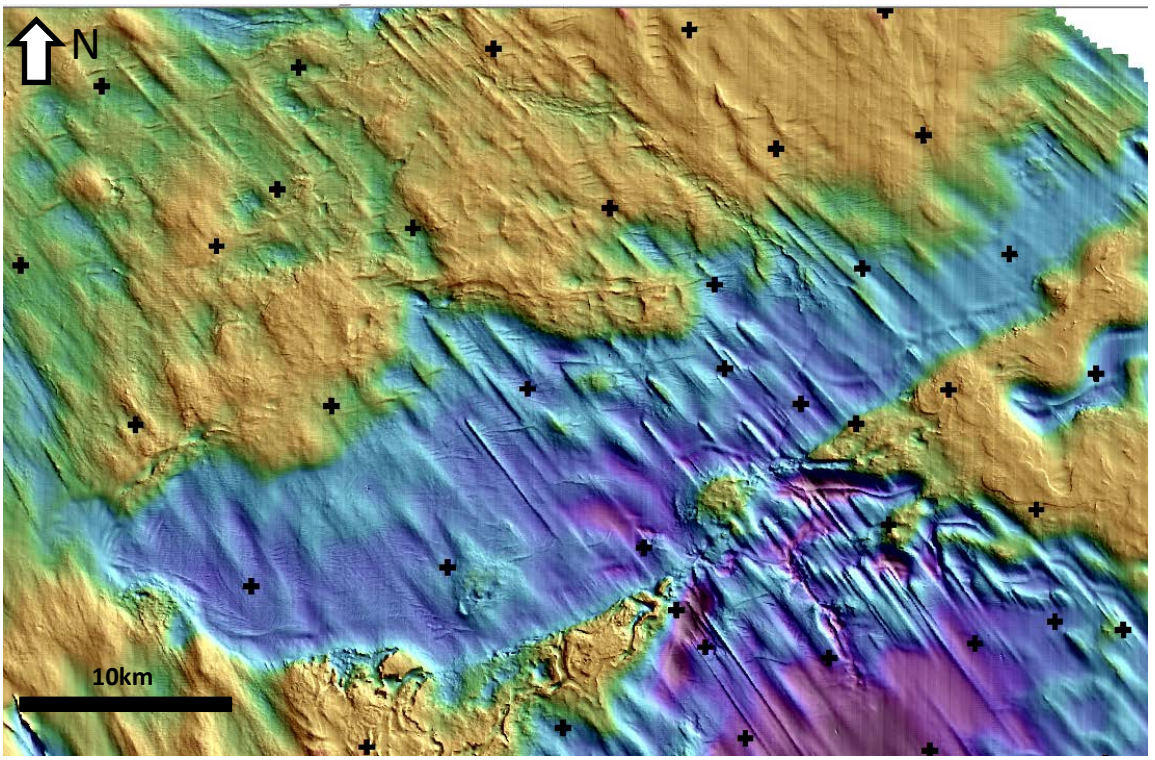

Fig. 12

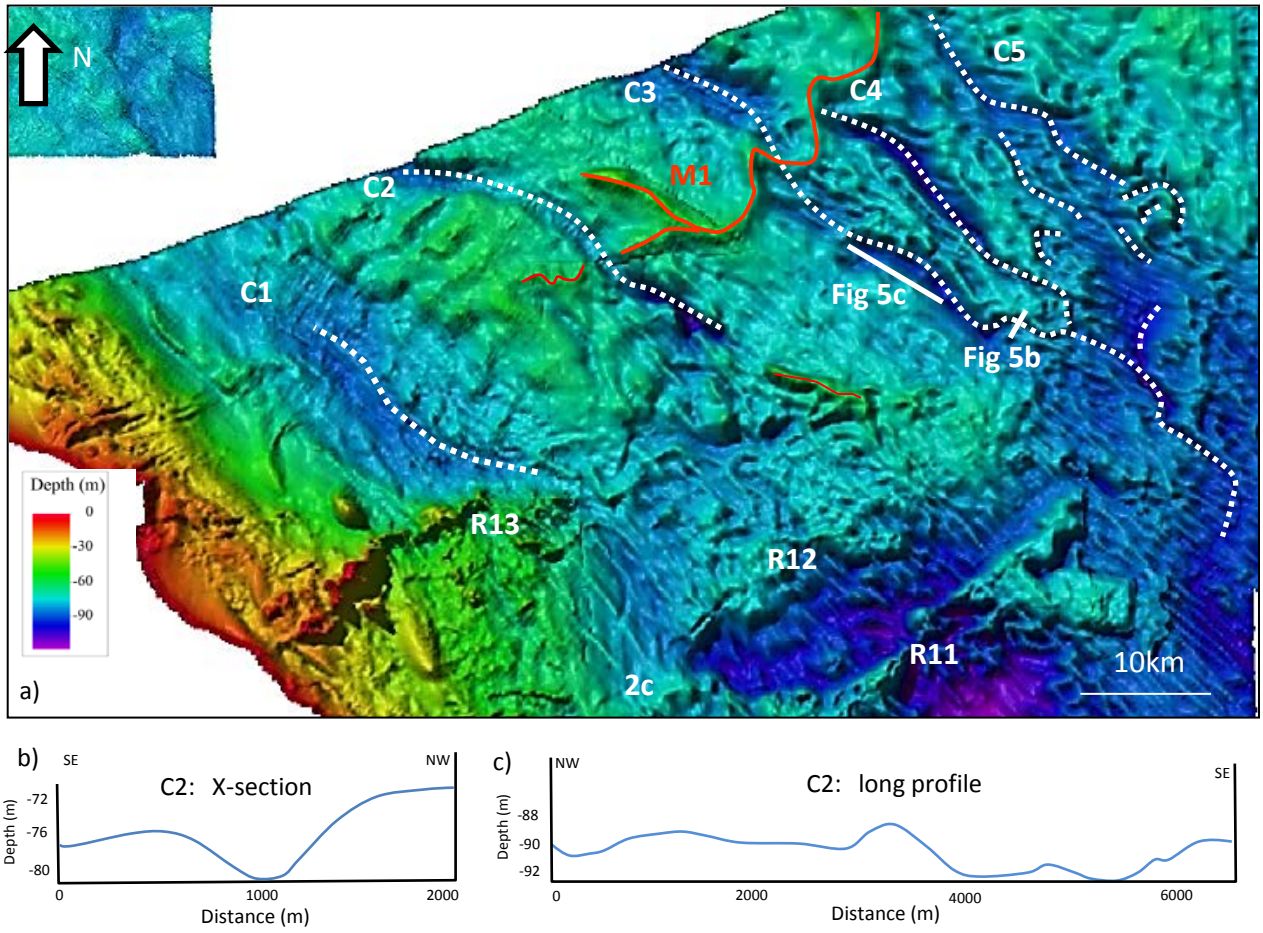
N
C1
C2
C3
C4
C5
M1
Fig 5c
Fig 5b
R13
R12
R11
2c
10km
Depth (m)
0
-30
-60
-90
a)
b)
SE
NW
C2: X-section
Depth (m)
-72
-76
-80
0
1000
2000
Distance (m)
c)
NW
SE
C2: long profile
Depth (m)
-88
-90
-92
0
2000
4000
6000
Distance (m)

Fig. 13

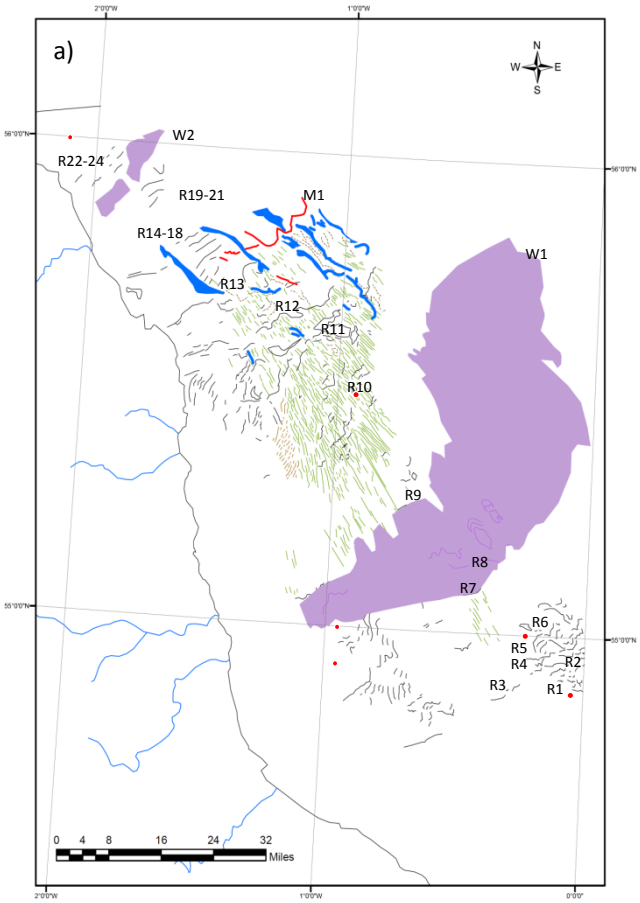
a)
N
W
E
S
W2
R22-24
R19-21
M1
R14-18
W1
R13
R12
R11
R10
R9
R8
R7
R6
R5
R4
R2
R3
R1
0 4 8 16 24 32
Miles

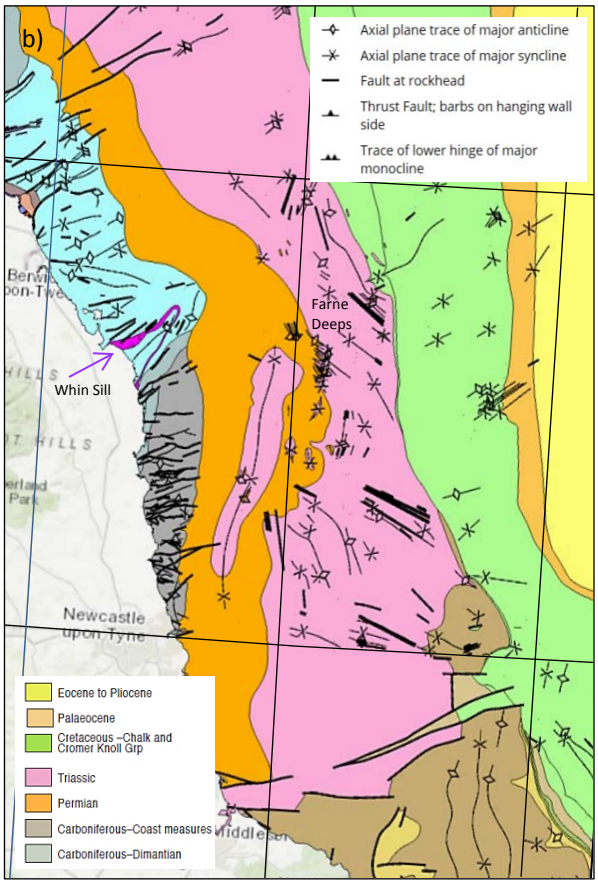
b)
Axial plane trace of major anticline
Axial plane trace of major syncline
Fault at rockhead
Thrust Fault; barbs on hanging wall side
Trace of lower hinge of major monocline
Farne Deeps
Whin Sill
Newcastle upon Tyne
Eocene to Pliocene
Palaeocene
Cretaceous –Chalk and Cromer Knoll Grp
Triassic
Permian
Carboniferous–Coast measures
Carboniferous–Dimantian

Fig. 14

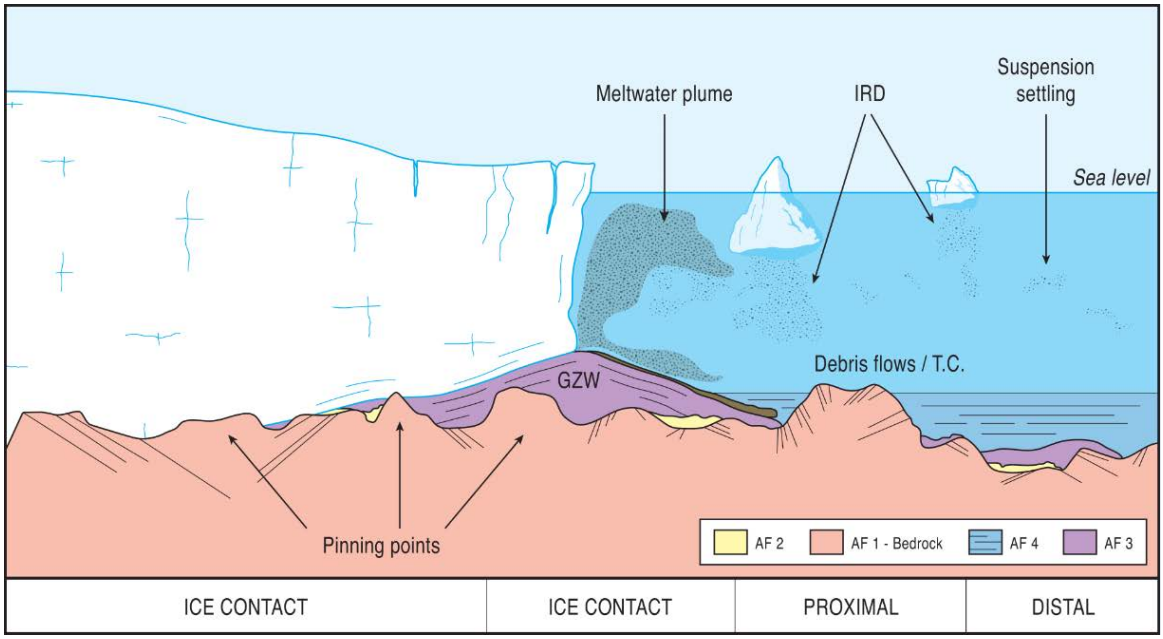
Meltwater plume
IRD
Suspension
settling
Sea level
Debris flows / T.C.
GZW
Pinning points
AF 2
AF 1 - Bedrock
AF 4
AF 3
ICE CONTACT
ICE CONTACT
PROXIMAL
DISTAL

Fig. 15

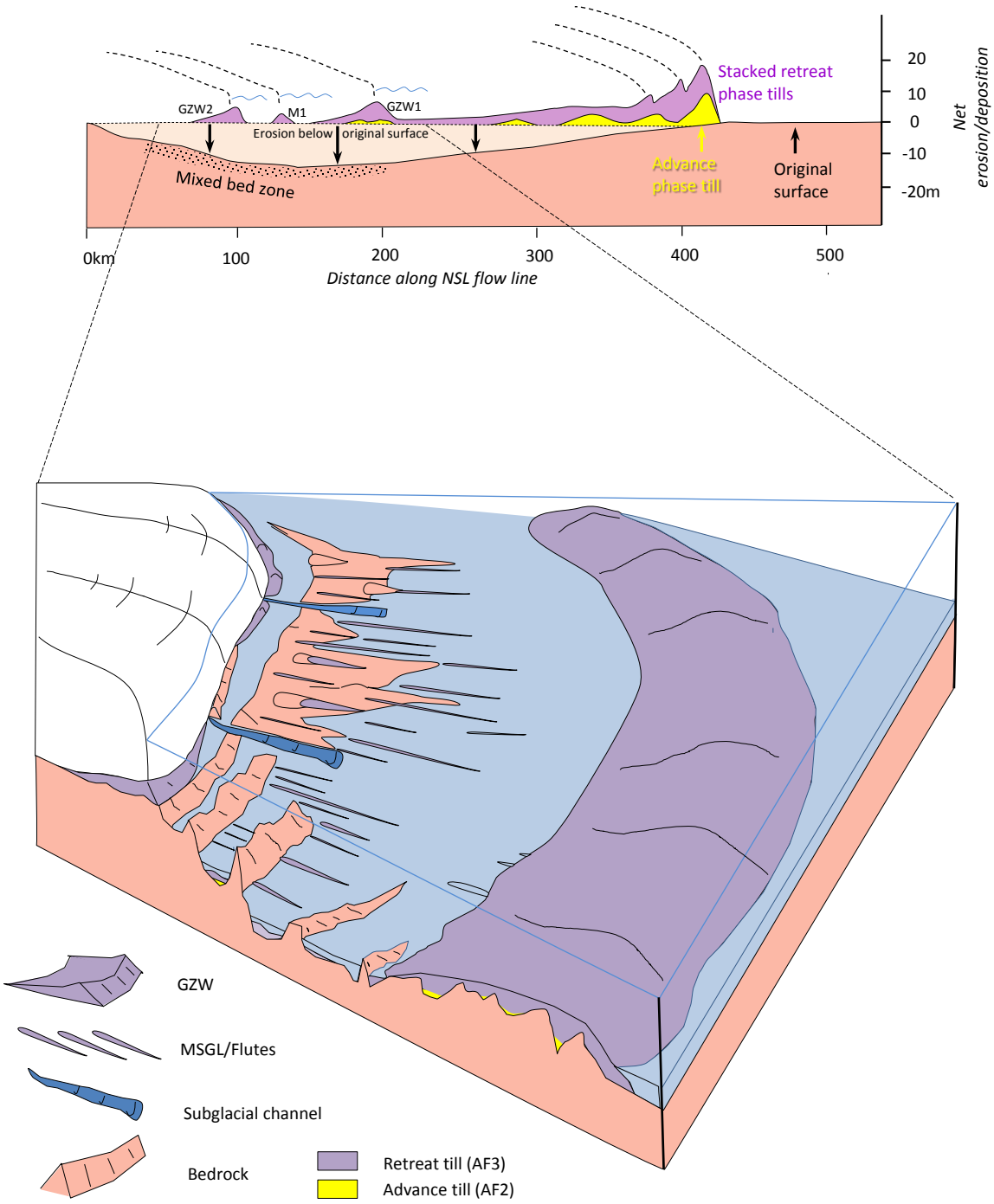
GZW2
M1
GZW1
Erosion below original surface
Mixed bed zone
Stacked retreat phase tills
Advance phase till
Original surface
20
10
0
-10
-20m
Net erosion/deposition
0km
100
200
300
400
500
Distance along NSL flow line
GZW
MSGL/Flutes
Subglacial channel
Bedrock
Retreat till (AF3)
Advance till (AF2)

Fig. 16

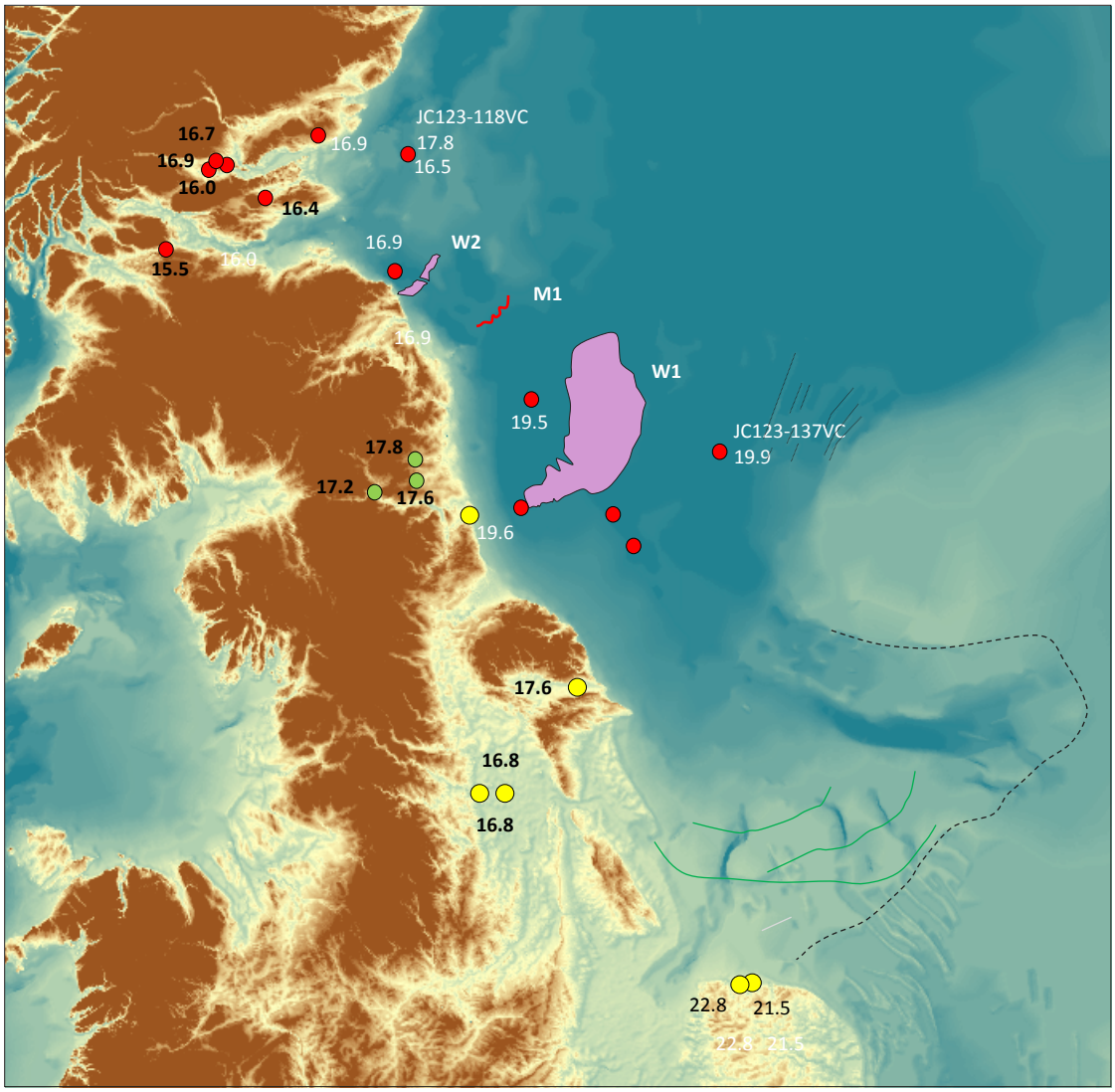
JC123-118VC
16.7
16.9
16.9
17.8
16.5
16.0
16.4
16.9
W2
15.5
16.0
M1
16.9
W1
19.5
JC123-137VC
19.9
17.8
17.2
17.6
19.6
17.6
16.8
16.8
22.8
21.5
22.8
21.5

Fig. 17